Fig. 3 Characterization of BNC displaying EC-Fc. (**A**) Schematic representation of the multivalent display of EC-Fc on ZZ-BNC (EC-Fc/BNC) and Fc on ZZ-BNC (Fc/BNC). (**B**) The solubility of BNC-displaying Fc/BNC and IgG/BNC was evaluated with FITC-labelled BNC. Residual fluorescence in supernatant was measured in varying molecular ratio of Fc or human IgG to ZZ-BNC. The intensity from the FITC-labelled ZZ-BNC without Fc was calculated as 1 in each graph. (**C**) Western blot analysis of Fc in the supernatant obtained in (**B**). Fc/BNC in the supernatant was immunoprecipitated with anti-HBsAg antibody conjugated to micro beads and was subjected to Western blotting. The Fc on the blot was detected with anti-human IgG. The bands were densitometrically analysed with ImageJ and relative intensity of each lane was plotted. (**D–F**) Assessment of internalization of EC-Fc/BNC in SK-BR-3 cells through Western blot. (**D**) EC-Fc/BNC (40 nM/2 nM) or Fc/BNC (40 nM/2 nM) was incubated with SK-BR-3 cells for 5 hrs at 4°C and 37°C. (**E**) SK-BR-3 cells were treated with various concentration of EC-Fc/BNC from 1 to 10 nM. Fc/BNC in 10 nM was taken as control. (**F**) SK-BR-3 cells were treated with 2 nM EC-Fc/BNC at various time periods. Simultaneously 2 nM Fc/BNC was taken as control. (**D–E**) After the incubation the cells were trypsinised and lysed followed by immunoprecipitation with anti-HBsAg antibody conjugated to micro beads. The precipitates were immunoblotted and were detected with anti–pre-S1 antibody. The bands of BNC were densitometrically analysed by ImageJ and plotted into each graph to evaluate amount endocytosed. (**G, H**) Confocal microscopic observation of SK-BR-3 cells treated with EC-Fc/BNC or Fc/BNC. Cells were incubated for various time periods (**G**) and for 4 hrs (**H**). The RITC-labelled ZZ-BNC was used and the cells were fixed and permeabilized. EC-Fc or Fc were detected with anti-human IgG labelled with FITC (**G**) and ErbB2 was detected with sc-08 antibody followed by rabbit anti-mouse IgG Alexa 488 (**H**). Bars, 10 μm.

together with BNC in SK-BR-3 whereas the Fc/BNC did not show any detectable internalization of ErbB2 as well as for BNC. As the result, the internalization of ErbB2 is concluded to be dependent on the uptake of BNC displaying EC-1 peptide multivalently. Internalization of EC-Fc/BNC was found to be dependent on both time course and ErbB2 in SK-BR-3 cells. Simultaneously, the internalization of ErbB2 was confirmed to be induced when EC-Fc/BNC was added. This observation implies that the cellular uptake of EC-Fc/BNC should be associated with the receptor-mediated endocytosis.

Comparative study of the effect by EC-Fc and EC-Fc/BNC

The specific binding of EC-1 ligand to cells overexpressing ErbB2 was assessed by immunostaining (Fig. 4A). Three cell lines MCF-7, SK-BR-3 and SK-OV-3 cells were selected and the binding of EC-Fc protein and EC-Fc/BNC was evaluated. The expression level ErbB2 was approximately 10^4 sites/cell in MCF-7 [30], 10^6 sites/cell in SK-BR-3 and SK-OV-3, respectively [31, 32]. The cells were incubated with EC-Fc or Fc or EC-Fc/BNC or Fc/BNC for 1 hr at 37°C followed by staining with anti-human IgG Fc-labelled with FITC. The fluorescence was observed only at the linage of SK-BR-3 and SK-OV-3 cells but not with MCF-7 whereas Fc and Fc/BNC did not show any positive staining in all cell lines. No detectable fluorescence at the confocal microscopy to MCF-7 attributes to the low ErbB2 expression in the cells. The surface binding of the EC-Fc/BNC as well as EC-Fc was then qualitatively analysed by flow cytometry. As shown in Figure 4A in SK-BR-3 and SK-OV-3 cells, EC-Fc (green line) as well as Ec-Fc/BNC (blue line) exhibited to bind to cell surface specifically. The binding efficiency of EC-Fc was found to be better than EC-Fc/BNC for SK-BR-3 cells. As the results, the specific binding of EC-Fc and EC-Fc/BNC to ErbB2 and overexpressing cells was successfully demonstrated.

ErbB2 internalization depending on the doses of EC-Fc and EC-Fc/BNC was assessed in the range of 20–200 nM in SK-BR-3 cells (Fig. 4B). ErbB2 internalization was observed with both EC-Fc and EC-Fc/BNC. When the intensity of the band analysed densitometrically showed the internalization of ErbB2 was more efficient by the stimulation for 2 hrs up to 100 nM of the ligand multivalently displayed on BNC than by EC-Fc ligand alone (Fig. 4C).

EC-Fc/BNC internalized through GEEC pathway in SK-BR-3 cells

Cells adopt divergent pathways for the endocytosis of the cargos and receptors. The key pathways were categorized into clathrin-dependent and clathrin-independent mechanisms [33]. The clathrin-independent pathway is further classified into caveolar and GPI-anchored early endocytic compartments (GEEC) pathways [33, 34]. ErbB2 is thought to be internalizing in SK-OV-3 through clathrin-mediated internalization [24]. In this study we found that the mechanism of internalization of ErbB2 present in SK-OV-3 cells is deficient in SK-BR-3 cells. We tried to identify the difference between the two cell lines using DNA microarray (Fig. S2). As a result the expression of claudin 16, caveolin-1 and caveolin-2 were found to be extensively down-regulated in SK-BR-3 cells when compared to SK-OV-3 cells. This absence of caveolin-1 in SK-BR-3 cells was further confirmed by immunostaining using anti-Cav1 antibody (Fig. 5A). SK-BR-3 did not show the presence of caveolin-1 suggesting that the impaired caveolar mechanism prevailing in the cell, which was consistent with the finding by the previous reports [13, 35]. Because caveolin-1 was detected in SK-OV-3 cells the internalization pathway deficient in SK-BR-3 cells might be attributed to caveolae.

The mechanistic approach for the uptake of the EC-Fc/BNC was assessed in SK-BR-3 cells using inhibitors for other pathways. SK-BR-3 cells were treated with EC-Fc/BNC in the presence or absence of inhibitors for clathrin, and GEEC pathway and the internalization was assessed. When the cells were treated with 100 nM CPZ, an amphiphilic drug, which inhibits the clathrin-mediated pathway, the internalization of the EC-Fc/BNC was unaffected (Fig. 5B).

© 2011 The Authors
Journal of Cellular and Molecular Medicine © 2011 Foundation for Cellular and Molecular Medicine/Blackwell Publishing Ltd

Most of the cargos irrespective of their route merges with Rab5 and early endosome antigen-1 (EEA-1) enriched in early endosomes, which is further sorted into various intracellular destinations [36, 37]. The colocalization of EC-Fc/BNC with EEA-1 was assessed with anti–EEA-1 antibody under confocal microscope at various time periods starting from 5, 30 and 90 min and the colocalization was found to be maximum at 30 min (Fig. S3).

When the cells were treated with 5 mM mβCD, which dislodges the cholesterol from the surface and inhibit the cdc42 activity, for 30 min the internalization was blocked and the cells untreated showed considerable uptake of EC-Fc/BNC. The bound fractions of EC-Fc/BNC were treated with and without acid stripping to ensure the colocalized fraction inside the cells (Fig. 5C). The colocalization was calculated to more than 60%, which was reduced in the internalization of EC-Fc/BNC with the mβCD treatment. To assess the surface binding of the EC-Fc/BNC after the inhibitor treatment the cells were stained for the ErbB2 and EC-Fc/BNC at various concentration of the mβCD (Fig. S4). The inhibitor treatment did not deteriorate the binding affinity of the EC-Fc/BNC to ErbB2. These results were further confirmed with flow cytometric studies (Fig. S5).

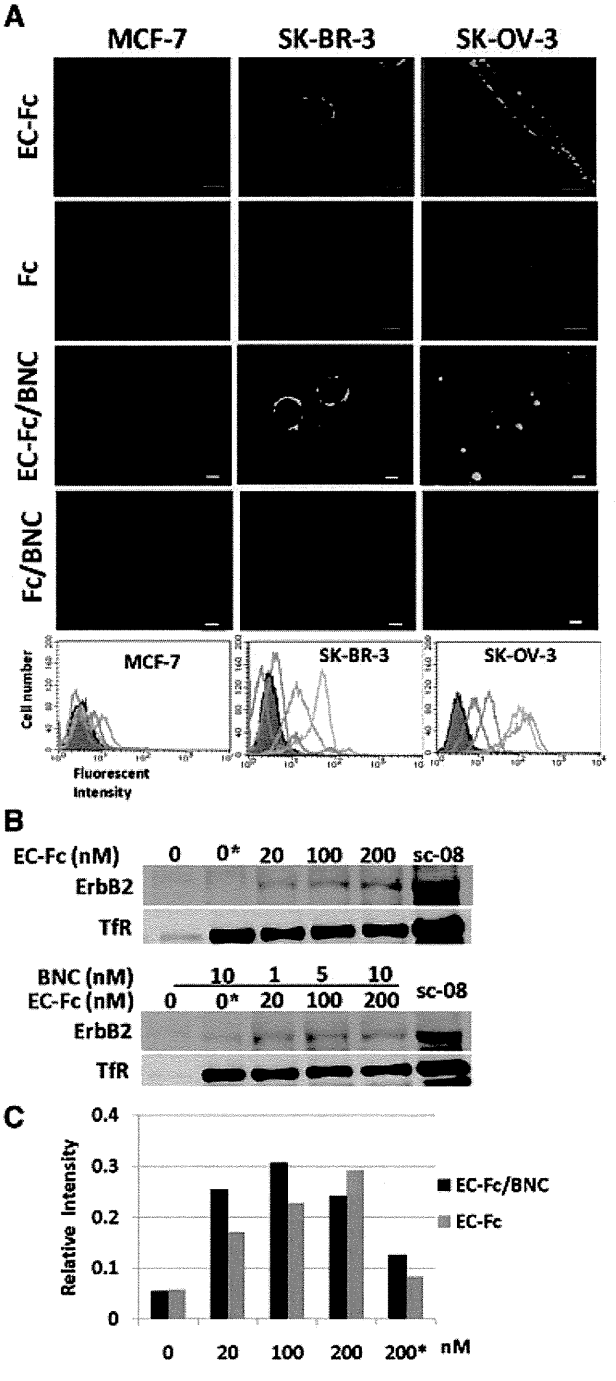

Fig. 4 Evaluation of ErbB2 internalization in SK-BR-3 cells treated with EC-Fc/BNC. (**A**) Comparison of EC-Fc/BNC bound to the surface of the cells over expressing ErbB2. Cells were incubated with EC-Fc (1 μM), Fc (1 μM), EC-Fc/BNC (40 nM/2 nM), and Fc/BNC (40 nM/2 nM) for 1 hr at 37°C in MCF-7 cells, SK-BR-3 cells, and SK-OV-3 cells. MCF-7 cells were used as the control for low ErbB2 expression. The cells were stained with anti-human IgG labelled with FITC. Bars depict 10 μm. The treated cells were also subjected to flow cytometoric analysis for the surface bound fraction of EC-Fc and Fc ligand with and without BNC in MCF-7, SK-BR-3 and SK-OV-3, respectively. Untreated cells were shown in shadow (grey). Treatment with EC-Fc ligand Fc ligand, EC-Fc/BNC and Fc/BNC was marked as green, magenta, blue and orange, respectively. (**B**) SK-BR-3 cells were treated with different concentration of EC-Fc or Ec-Fc/BNC. The cell surface receptors were reversibly biotinylated with NHS-SS-Biotin and were incubated with EC-Fc, Fc, EC-Fc/BNC or Fc/BNC for 2 hrs at 37°C. SK-BR-3 cells left untreated at 4°C for 2 hrs were shown as lane '0'. '0*' corresponds to the cells treated with Fc ligand (top) and Fc/BNC (lower) at a concentration of 200 nM, respectively. After the treatments, cells were lysed, immunoprecipitated with avidin agarose and were subjected to Western blot to detect ErbB2 with anti-ErbB2 antibody. sc-08 antibody treatment was taken as positive control for endocytosis of ErbB2. Transferrin receptor (TfR) was monitored as an internal control for the experiments. (**C**) The bands from the Western blots were densitometrically analysed with ImageJ and the intensity each band was normalized by the intensity when treated with antibody sc-08.

Discussion

The EC-Fc was designed as dimer due to the hinge region in IgG Fc domain (Fig. 1A). However, we found higher oligomeric forms such as tetramer and hexamer. These higher order forms were supposed to be divalent as described in 'Results' and Figure 1C. Further multivalent form of EC-1 peptide was prepared by displaying EC-Fc on BNC which was optimized to a ratio of EC-Fc to BNC = 1:20. These divalent and multivalent forms of EC-Fc induced internalization of ErbB2 into SK-BR-3 cells whereas

© 2011 The Authors
Journal of Cellular and Molecular Medicine © 2011 Foundation for Cellular and Molecular Medicine/Blackwell Publishing Ltd

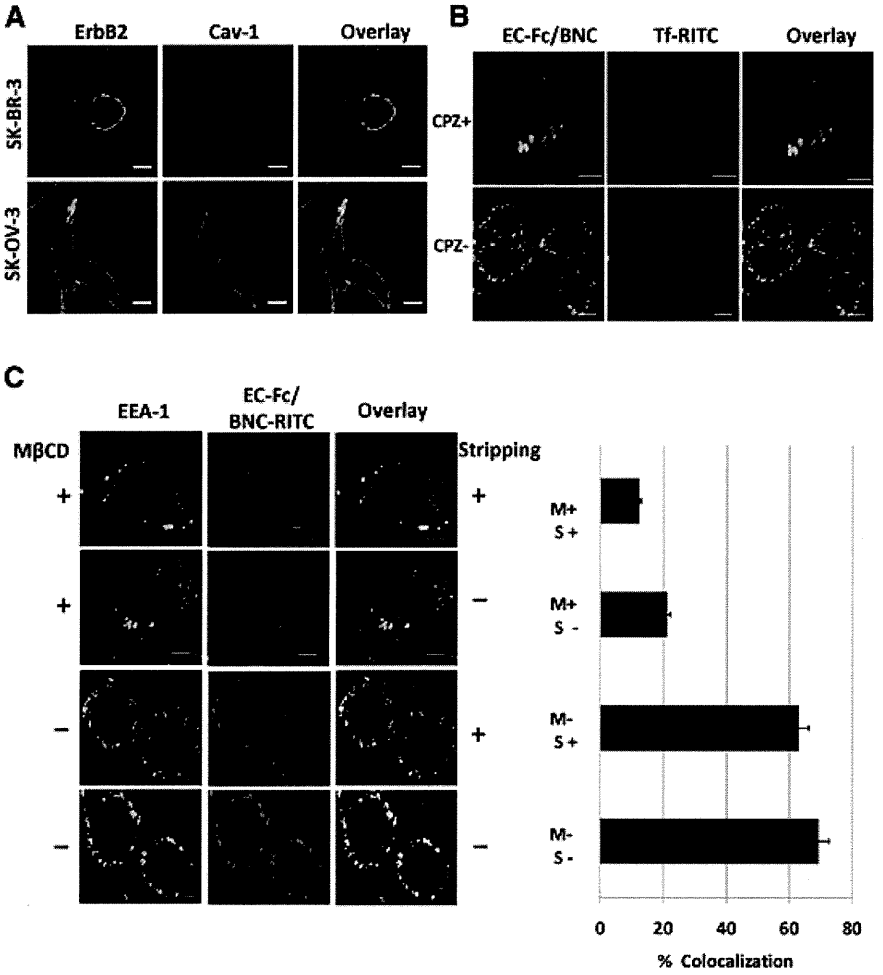

Fig. 5 Assessment of the mechanism of internalization of EC-Fc/BNC in SK-BR-3 cells. (**A**) SK-BR-3 cells and SK-OV-3 cells were stained with antibodies against ErbB2 (green) and Cav-1 (red). (**B**) SK-BR-3 cells were treated with EC-Fc/BNC in the presence or absence of 100 nM of CPZ and stained with anti-human IgG antibody labelled with FITC. Transferrin-RITC was used as a control for the internalization. (**C**) SK-BR-3 cells were treated with EC-Fc/BNC labelled with RITC in the presence or absence of mβCD. The cells were stained with anti–EEA-1 antibody followed by secondary antibody against mouse IgG labelled with AlexaFlour-488. The cells were then stripped with and without acid treatment to remove the surface bound fraction and to visualize the internalized fraction. Bars, 10 μm.

monovalent form of EC-1 peptide did not induce internalization [24]. The internalization of ErbB2 was found dependent on the concentration in the range of 20–200 nM for EC-Fc and appeared to be enhanced when 20–100 nM EC-Fc was displayed on BNC (Fig. 4B). EC-Fc/BNC appeared more efficient in inducing the internalization of ErbB2 when compared to EC-Fc ligand alone. The time course dependence of the BNC internalization was found to be also in the same range of EC-Fc/BNC concentration. The binding affinity of the EC-Fc was estimated to be about 26 nM whereas monovalent EC-1 peptide as EC-eGFP fusion showed 1 μM (Table 1). The affinity of the multivalent display for ErbB2 was 33 nM, which did not ameliorate the affinity of EC-Fc for the ErbB2. Therefore, the affinity should elucidate the enhanced internalization of ErbB2 induced by EC-Fc/BNC in SK-BR-3 cells. It is believed that the heterodimerization between ErbB2 and ErbB3 is one of the reasons for retention of ErbB2 on the cell surface, so that monovalent form of the EC-1 peptide could not induce internalization of ErbB2 in SK-BR-3 cells. Shuttling between homodimers and heterodimers should increase depending on the distance of the dimers. EC-Fc supposedly keeps the receptors close enough to facilitate homodimer formation, which will allow the internalization of ErbB2. Therefore, the cells treated with EC-Fc/BNC showed considerable increment in the internalization of

Table 1 Affinity for ErbB2 of EC-1 peptide in various forms and internalization of ErbB2 in SK-OV-3 and SK-BR-3 cells

Forms of EC-1 peptide	EC-eGFP	EC-Fc	EC-Fc/BNC
Kd (nM)	1.0×10^{3}*	2.6×10	3.3×10
Internalization of ErbB2 observed in			
SK-OV-3 cells	+†	++‡	++
SK-BR-3 cells	–§	+	++

*[24].
†Internalization was observed in the range of μM orders of ligands.
‡Internalization was observed in the range of nM orders of ligands.
§Internalization was not observed.

© 2011 The Authors
Journal of Cellular and Molecular Medicine © 2011 Foundation for Cellular and Molecular Medicine/Blackwell Publishing Ltd

the BNC, although the effect of EC-Fc moiety appeared conceivable because Fc/BNC did not show significant internalization of ErbB2 as the background (Fig. 3D–F).

It is thought that the processing and degradation of the ErbB2 is different in various cell lines [24, 34, 35]. The CPZ at 100 nM, which inhibits the formation of clathrin-coated pits, inhibited the internalization of ErbB2 by EC-1 peptide fused to eGFP in SK-OV-3 [24]. On the contrary, the same concentration of CPZ did not block the internalization of ErbB2 in SK-BR-3 cells. In this study, we confirmed the absence of caveolin-1 in SK-BR-3 cells using microarray and immunostaining where it showed around 300-fold increment in the expression of Cav-1 in SK-OV-3 cells (Fig. S1). Recent studies support our observation that the SK-BR-3 cells lack caveolae [13, 35]. ErbB2 internalization after geldanamycin treatment showed GEEC or clathrin-independent compartments (CLIC) pathway, which ultimately fuses with the classical pathway for the degradation in lysosomes, is independent of caveolar and clathrin pathway [35].

In this study we employed mβCD, a cholesterol dislodging oligosaccharide, for deciphering the mechanism behind the internalization of the EC-Fc/BNC in SK-BR-3 cells, as an inhibitor for the blockade of GEEC pathway. Cholesterol depletion with mβCD inhibits both caveolar [38] and GEEC pathway [39, 40]. Earlier it was shown that cholesterol level determines the internalization of GPI-anchored proteins and with clostridium difficile toxin B [34, 39]. Because SK-BR-3 cells lack caveolar machinery, the blockade with mβCD will only correspond its effect in blocking the internalization of GEEC-mediated mechanism. The internalization of ErbB2 is sensitive to the depletion of cholesterol, which is essential for most of the clathrin-independent pathways. GEECs are formed as compartments free of clathrin, caveolin and dynamin, which are short lived (2–5 min) and ultimately fuses with EEA-1 enriched early endosome [33, 38]. It was shown that cdc42 is responsible for the dynamin-dependent and clathrin-independent internalization of GPI-anchored proteins. It was also reported earlier that cdc42 activation recruits actin polymerization machinery rendering this pathway sensitive to inhibitors of cholesterol depletion and actin polymerization [39]. This pathway specifies the visible difference in the uptake of the EC-Fc/BNC between SK-OV-3 and SK-BR-3 cells.

Another important molecule, which plays a key role in the GEEC pathway, is EEA-1 that contains an FYVE finger, which interacts with PI3K [41, 42]. PI3K phosphorylates Rab 5 that helps the EEA-1 to localize to early endocytic compartments [36]. The colocalization of EC-Fc/BNC with EEA-1, which corresponds the preliminary step in the endosomal pathways before transferring it to the sorting endosomes, was observed (Fig. S2). Because both caveolar and clathrin pathways are impaired in SK-BR-3 cells as described earlier, the colocalization should correspond to GEEC pathway.

In this study, we revealed the presence of GEEC pathway as ErbB2 internalization, which critically differs between SK-BR-3 cells and SK-OV-3 cells using EC-1 peptide in various forms. As for the nanoparticle internalization, the pathways of clathrin and caveolar- independent endocytosis have not been described until now [43]. The internalization of the carrier particle was described repeatedly on folate receptor (FR) tagged nanoparticles [44]. In these reports, mechanism of the carrier internalization emphasizes the FR internalization through GEEC pathway. Similarly, EC-Fc should utilize the mechanism of internalization of ErbB2 in this study even when they are displayed on BNC (Fig. 4B).

It is considered that ZZ-BNC is an efficient nano-machine for molecular targeting in drug delivery system displaying antibodies on the surface [25, 29, 45]. Multivalency of EC-Fc was successfully demonstrated to target ErbB2 enhancing the internalization of ErbB2, in this report. In this context, delivery of therapeutic substances into specific cells of various diseases including cancer can be feasible if EC-Fc/BNC is used as a drug delivery system. Multivalent display strategy proposed here should be useful for molecular targeting to introduce therapeutic drug into the cells followed by the internalization of receptors.

Acknowledgements

The authors thank Prof. N. Kanayama for his valuable help and suggestions in flow cytometric analysis. The authors also thank Prof. H. Matsui for helpful discussion throughout the work. This work was partly supported by Grant-in-Aid for Scientific Research (B) from the Ministry of Education, Culture, Sports, Science and Technology (No. 21300179) in Japan, Health and Labor Sciences Research Grants, Research on Nanotechnical Medical, H21-nano-general-004 and National Natural Science Foundation of China (Key Program, Grant No. 30930038).

Conflict of interest

The authors report no conflicts of interest. The authors alone are responsible for the content and writing of the paper.

Supporting information

Additional Supporting Information may be found in the online version of this article:

Fig. S1 Live cell imaging. For live cell imaging, the SK-BR-3 cells were cultured in 18 mm coverslips and washed twice with phenol red free RPMI (Sigma) containing 1 % glucose, 25 mM HEPES and 1 % BSA supplemented with 100 U/ml pencillin and 100 μg/ml streptomycin. The EC-Fc BNC tagged with RITC was incubated on ice for 30 min prior to the visualization in order to enable the binding of the multivalent forms of BNC to the cell surface. The cells were then washed thrice with warm media and were visualized in 100X 1.3 N.A. oil immersion objectiveunder Olympus IX81 inverted microscope (Olympus) with temperature control followed by data acquisition with Metamorph software (Molecular Devices). The imaging was carried out with DP71 cooled CCD camera attached to the microscope and the fluorescence of RITC was acquired along with the DIC field image. The time-lapse imaging

© 2011 The Authors
Journal of Cellular and Molecular Medicine © 2011 Foundation for Cellular and Molecular Medicine/Blackwell Publishing Ltd

was carried out for one hour with time intervals of 5 minutes each. In Metamorph software, each channel was split and overlayed separately. The acquired stacks were analyzed with MBF Image J.

Fig. S2 Microarray analysis. Expression of genes in SK-BR-3 cells was analyzed by microarray procedure. Total RNA preparation and analysis was performed as described previously [46, 47]. DNA microarray was carrying 1,795-oligonucleotide probes for human cell surface proteins. cDNAs were synthesized with Superescript II reverse transcriptase (Invitrogen) with oligo dT primers. Amino-allyl-dUTP was incorporated into cDNAs followed by coupling with Cy-3 dye (Ambion, TX, USA) and were processed for hybridization at 55°C for 15 hours. The fluorescent images for the hybridization were captured using FLA8000 scanner (Fuji Film, Japan) and analyzed with GenePix Pro5.1 software (Axon Instruments, CA). We found caveolins, Cav-1 and 2, and claudin 16 (CLDN-16) were downregulated in SK-BR-3 cells when compared to SK-OV-3 cells while ErbB2 and GAPDH expression were equally expressed in both the cell lines. RT-PCR (Fig. S1A) and qRT-PCR (Fig. S1B) further confirmed these results. The conditions for the RT-PCR are as follows: 94°C for 5min; followed by 30 cycles of 94°C for 30 sec, 55°C for 30 sec, 72°C for 30 sec and 72°C for 7 minutes. Quantitative real time PCR was performed with SYBR Green Realtime Master Mix (Toyobo) in triplicates containing 5ng of cDNA along with 400 nM primers using LightCycler™ (Roche). The thermal cycling condition was as follows: 95°C for 1 min followed by 40 cycles of 95°C -10 sec, 55°C for 10 sec, 72°C for 25 sec and 60°C for 1 min. The following sets of the primers were used for the PCR reaction. Claudin-16, (Forward) 5′- GCTTGCCACAATGAGGGATCT-3′, (Reverse) 5′-TGACTTGGCCATGGAAACACC-3′; Cav-1 (Forward) 5′-GACTCG-GAGGGACATCTCTAC-3′, (Reverse) 5′-GTTGATGCGGACATTGCTGA-3′; Cav-2, (Forward) 5′-ACGTACAGCTCTTCATGGAC-3′ (Reverse) 5′-CAGTTGCAGGCTGACAGAAG-3′.

Fig. S3 Time dependent colocalization of EC-Fc BNC in early endosomes. Colocalization of EC-Fc/BNC-RITC with EEA-1 was found in the early endosomes. SK-BR-3 cells were treated with EC-Fc/BNC-RITC for 5, 30, 90 min, and the colocalization of the EC-Fc/BNC-RITC with the early endosomal marker, EEA-1 was assessed with anti EEA-1 antibody (BD Biosciences) and the secondary antibody labeled with AlexaFlour-488 (Molecular Probes). Error bars indicate standard error. JACoP plugin in Image J was employed for percentage colocalization assessment. Percentage colocalization was found to be maximum up to approximately 70% by 30 min. The data represented here is the representative of two independent experiments.

Fig. S4 Binding of EC-Fc BNC to the cell surface after treatment with varying concentration of mβCD. The binding of EC-Fc/BNC's to ErbB2, in the presence of 2 to 10 mM of cholesterol dislodging oligosaccharide-mβCD, was not affected. SK-BR-3 cells were treated with 5 and 10 mM of mβCD for 30 minutes followed by treatment with EC-Fc/BNC labeled with RITC are shown in Figure S2. The cells were stained with anti ErbB2 antibody (green) and red spots indicate EC-Fc/BNC labeled with RITC. Bars depict 10 μm.

Fig. S5 FACS analysis for the surface binding and internalization of EC-Fc BNC with inhibitor treatment. Surface binding and internalization of EC-Fc/BNC labeled with FITC in SK-BR-3 cells was quantified using FACS analysis. First, the binding of EC-Fc/BNC on SK-BR-3 cells was treated with or without 5 mM of mβCD on ice for 30 min. The cells were then fixed and analyzed with FACS to determine the surface bound fraction (Fig. S5A). The histograms showed overlapping of the peak tops indicating that the surface binding is majorly unaffected by the mβCD treatment. The peak (blue), which corresponds to approximately 20% of the total cell counts, orienting towards the untreated cells (grey peak) indicates the presence of a different population of cells that are incapable of binding to EC-Fc/BNC after mβCD treatment. Simultaneously, another set cells were treated with EC-Fc/BNC labeled with FITC in the presence or absence of 5 mM of mβCD at 37°C for 30 minutes. Cells were then trypsinized to remove the surface fraction, fixed and permeabilized, and the internalized fraction was analyzed adopting the same procedure with FACS (Fig. S5B, C). mβCD treated SK-BR-3 cells showed a peak point in the histogram which overlaid the peak area of untreated cells indicating the mβCD inhibits the internalization, while the cells without mβCD treatment drifted from the untreated cells towards the right. Total intensity of the internalized fraction was assessed from the FACS data were plotted on to a graph (Fig. S5). mβCD suppressed the internalization to approximately 50% when compared to the absence of mβCD treatment. M: mβCD; T: trypsin. Error bars indicate standard error.

Please note: Wiley-Blackwell is not responsible for the content or functionality of any supporting information supplied by the authors. Any queries (other than missing material) should be directed to the corresponding author for the article.

References

1. **Yarden Y, Sliwkowski MX.** Untangling the ErbB signaling network. *Nature Rev Mol Cell Biol.* 2001; 2: 127–37.
2. **Olayioye MA, Neve, RM, Lane HA, *et al.*** The ErbB signaling network: receptor heterodimerization in development and cancer. *EMBO J.* 2000; 9: 3159–67.
3. **Klapper LN, Waterman H, Sela M, *et al.*** Tumor-inhibitory antibodies to HER-2/ErbB-2 may act by recruiting c-Cbl and enhancing ubiquitination of HER-2. *Cancer Res.* 2000; 60: 3384–8.
4. **Slamon DJ, Clark GM, Wong SG, *et al.*** Human breast cancer: correlation of relapse and survival with amplification of the HER-2/neu oncogene. *Science.* 1987; 235: 177–82.
5. **Hynes, NE, Stern DF.** The biology of ErbB2/neu/HER-2 and its role in Cancer. *Biochem Biophys Acta.* 1994; 1198: 164–84.

© 2011 The Authors
Journal of Cellular and Molecular Medicine © 2011 Foundation for Cellular and Molecular Medicine/Blackwell Publishing Ltd

6. **De Placido S, Carlamangno C, De Laurentiis M, *et al.*** C-erbB2 expression predicts tamoxifen efficacy in breast cancer patients. *Breast Cancer Res Treat.* 1998; 52: 55–64.
7. **Pinkas-Kramarski R, Soussan L, Waterman H, *et al.*** Diversification of Neu differentiation factor and epidermal growth factor signaling by combinatorial receptor interactions. *EMBO J.* 1996; 15: 2452–67.
8. **Baselga J, Swain SM.** Novel anticancer targets: revisiting ERBB2 and discovering ERBB3. *Nat Rev Cancer* 2009; 9: 463–75.
9. **Salomon DS, Brandt R, Ciardiello F, *et al.*** Epidermal growth factor-related peptide and their receptors in human malignancies. *Crit Rev Oncol Ematol.* 1995; 19: 183–232.
10. **Slamon DJ, Godolphin W, Jones LA, *et al.*** Studies of the HER-2/neu proto-oncogene in human breast and ovarian cancer. *Science.* 1989; 244: 707–12.
11. **Zhang X, Silva E, Gershenson D, *et al.*** Amplification and rearrangement of c-erb B proto-oncogenes in cancer of human female genital tract. *Oncogene* 1989; 4: 985–9.
12. **Austin CD, De Maziere AM, Pisacane PI, et al**. Endocytosis and sorting of ErbB2 and the site of action of cancer therapeutics trastuzumab and geldanamycin. *Mol Biol Cell.* 2004; 15: 5268–82.
13. **Hommelgaard AM, Lerdrup M, van Deurs B.** Association with membrane protrusions makes ErbB2 and internalization-resistant receptor. *Mol Biol Cell.* 2004; 15: 1557–67.
14. **Lerdrup M, Brunn S, Grandal MV, *et al.*** Endocytic downregulation of ErbB2 is stimulated by cleavage of its C-terminus. *Mol Biol Cell.* 2007; 18: 3656–66.
15. **Lerdrup M, Hommelgaard AM, Grandal MV, *et al.*** Geldanamycin stimulates internalization of ErbB2 in a proteosome-dependent pathway. *J Cell Sci.* 2006; 119: 85–95.
16. **Hudziak RM, Lewis GD, Winget M, *et al.*** P185HER2 monoclonal antibody has antiproliferative effects *in vitro* and sensitizes human breast tumor cells to tumor necrosis factor. *Mol. Cell. Biol.* 1989; 9: 1165–72.
17. **Lewis GD, Lofgren JA, McMurtey AE, *et al.*** Growth regulation of human breast and ovarian tumor cells by heregulin: evidence for the requirement of ErbB2 as a critical component in mediating heregulin responsiveness. *Cancer Res.* 1996; 56: 1457–65.
18. **Cuello M, Ettenberg SA, Clark AS, *et al.*** Downregulation of the erbB2 receptor by trastuzumab (herceptin) enhances tumor necrosis factor related apoptosis inducing ligand mediated apoptosis in breast and ovarian cancer cell lines that overexpress erbB2. *Cancer Res.* 2001; 61: 4892–900.
19. **Baselga J, Albanell J, Molina MA, *et al.*** Mechanism of action of trastuzumab and scientific update. *Semin Oncol.* 2001; 28: 4–11.
20. **Urbanelli L, Ronchini C, Fontana L, *et al.*** Targeted gene transduction of mammalian cells expressing the HER2/neu receptor by filamentous phage. *J Mol Biol.* 2001; 313: 965–76.
21. **Karasseva NG, Glinsky VV, Chen NX, *et al.*** Identification and characterization of peptides that bind human ErbB2 selected from a bacteriophage display library. *J Protein Chem.* 2002; 21: 287–96.
22. **Houimel M, Schneider P, Terskikh A, *et al.*** Selection of peptides and synthesis of pentameric peptabody molecules reacting specifically with ErbB-2 receptor. *Int J Cancer.* 2001; 92: 748–55.
23. **Pero SC, Shukla GS, Armstrong AL, *et al.*** Identification of a small peptide that inhibits the phosphorylation of ErbB2 and proliferation of ErbB2 overexpressing breast cancer cells. *Int J Cancer.* 2004; 111: 951–60.
24. **Hashizume T, Fukuda T, Nagaoka T, *et al.*** Cell type dependent endocytic internalization of ErbB2 with an artificial peptide ligand that binds to ErbB2. *Cell Biol Int.* 2008; 32: 814–26.
25. **Tsutsui Y, Tomizawa K, Nagita M, *et al.*** Development of bionanocapsules targeting brain tumors. *J Control Release* 2007; 122: 159–64.
26. **Tada H, Kurokawa T, Seita T, *et al.*** Expression and characterization of a chimeric bispecific antibody against fibrin and against urokinase-type plasminogen activator. *J Biotech.* 1994; 33: 157–74.
27. **Seno M, Futami J, Kosaka M, *et al.*** Nucleotide sequence encoding human pancreatic ribonuclease. *Biochim Biophys Acta.* 1994; 1218: 466–8.
28. **Nagaoka T, Fukuda T, Hashizume T, *et al.*** A betacellulin mutant promotes differentiation of pancreatic acinar AR42J cells into insulin-producing cells with low affinity of binding to ErbB1. *J Mol Biol.* 2008; 380: 83–94.
29. **Yamada T, Iwasaki Y, Tada H, *et al.*** Nanoparticles for the delivery of genes and drugs to human hepatocytes. *Nat Biotechnol.* 2003; 21: 885–90.
30. **Dini M, Jafari K, Faiferman I.** Cell-mediated cytotoxicity in pre invasive and invasive squamous cell carcinoma of the cervix. *Obstet Gynecol.* 1980; 55: 728–31.
31. **Hughes DPM, Thomas, DG, Giordano TJ, *et al.*** Cell surface expression of epidermal growth factor receptor and Her-2 with nuclear expression of Her-4 in primary osteosarcoma. *Cancer Res.* 2004; 64: 2047–53.
32. **Friedman LM, Rinon A, Schechter B, *et al.*** Synergistic down-regulation of receptor tyrosine kinases by combinations of mAbs: implications for cancer immunotherapy. *Proc Natl Acad Sci.* 2005; 102: 1915–20.
33. **Mayor S, Pagano RE.** Pathways of clathrin-independent endocytosis. *Nat. Rev. Mol. Cell. Biol.* 2007; 8: 603–12.
34. **Kirkham M, Parton RG.** Clathrin-independent endocytosis: new insights into caveolae and non-caveolar lipid raft carriers. *Biochim Biophys Acta.* 2005; 1745: 272–86.
35. **Barr DJ, Ostermeyer-Fay AG, Matundan RA, *et al.*** Clathrin-independent endocytosis of ErbB2 in geldanamycin-treated human breast cancer cells. *J Cell Sci.* 2008; 121: 3155–66.
36. **Sönnichsen B, De Renzis S, Neilsen E, *et al.*** Distinct membrane domains on endosomes in the recycling pathway visualized by multicolor imaging of Rab4, Rab5, and Rab 11. *J Cell Biol.* 2000; 149: 901–14.
37. **Falcone S, Cocucci E, Podini P, *et al.*** Macropinocytosis: regulated coordination of endocytic and exocytic membrane traffic events. *J Cell Sci.* 2006; 119: 4758–69.
38. **Sabharanjhak S, Sharma P, Parton RG, *et al.*** GPI-anchored proteins are delivered to recycling endosomems *via* a distinct cdc42-regulated, clathrin-independent pinocytic pathway. *Dev Cell.* 2002; 2: 411–23.
39. **Chadda R, Howes MT, Plowman SJ, *et al.*** Cholesterol-sensitive Cdc42 activation regulates actin polymerization for endocytosis *via* the GEEC pathway. *Traffic.* 2007; 8: 702–17.
40. **Brown FD, Rozelle AL, Yin HL, *et al.*** Phosphatidylinositol 4,5-bisphosphate and Arf6-regulated membrane traffic. *J Cell Biol.* 2001; 154: 1007–18.
41. **Mu F-T, Callaghan JM, Steele-Mortimer O, *et al.*** EEA1, an early endosome-associated protein. EEA 1 is a conserved alpha-helical peripheral membrane protein flanked by systeine "fingers" and contains a calmodulin-binding IQ motif. *J Biol Chem.* 1995; 270: 13503–11.
42. **Mills I, Jones A, Clague M.** Involvement of the endosomal autoantigen EEA1

© 2011 The Authors
Journal of Cellular and Molecular Medicine © 2011 Foundation for Cellular and Molecular Medicine/Blackwell Publishing Ltd

in homotypic fusion of early endosomes. *Curr Biol.* 1998; 8: 881–4.

43. **Sahay G, Alakhova YD, Kabanov VA.** Endocytosis of nanomedicines. *J. Con. Rel.* 2010; 145: 182–95.
44. **Lu Y, Low PS.** Folate mediated delivery of macromolecular anticancer therapeutic agents. *Adv Drug Deliv Rev.* 2002; 54: 675–93.
45. **Yu D, Fukuda T, Kuroda S, *et al.*** Engineered bio-nanocapsules, the selective vector for drug delivery system. *IUBMB Life.* 2006; 58: 1–6.
46. **Tuoya, Hirayama K, Nagaoka T, *et al.*** Identification of cell surface marker candidates on SV-T2 cells using DNA microarray on DLC-coated glass. *Biochem Biophys Res Commun.* 2005; 334: 263–8.
47. **Samah AS, Yuh Sugii, Tuoya, *et al.*** Identification of TM9SF2 as a candidate of the cell surface marker common to breast carcinoma cells. *Clin Oncol Cancer Res.* 2009; 6: 1–9.

© 2011 The Authors
Journal of Cellular and Molecular Medicine © 2011 Foundation for Cellular and Molecular Medicine/Blackwell Publishing Ltd

Journal of Controlled Release 149 (2011) 29–35

Contents lists available at ScienceDirect

Journal of Controlled Release

journal homepage: www.elsevier.com/locate/jconrel

Acylation of octaarginine: Implication to the use of intracellular delivery vectors

Sayaka Katayama, Hisaaki Hirose, Kentaro Takayama, Ikuhiko Nakase, Shiroh Futaki *

Institute for Chemical Research, Kyoto University, Uji, Kyoto 611-0011, Japan

ARTICLE INFO

Article history:
Received 18 November 2009
Accepted 1 February 2010
Available online 6 February 2010

Keywords:
Arginine-rich peptide
Cell-penetrating peptide
Fatty acid
Membrane interaction

ABSTRACT

Cell-penetrating peptides (CPPs) have the ability to efficiently internalize into cells and thus have been used as a vector for the intracellular delivery of various bioactive molecules. The introduction of a hydrophobic core to CPPs may increase their interaction with membranes and facilitate their translocation into cells. While the usefulness of acylated oligoarginine to gene and siRNA delivery has been largely reported, little information is available about their use for the delivery of small molecular-weight compounds, peptides and proteins. In this report, we employed octaarginine (R8) as a typical arginine-rich CPP and evaluated the effect of acylation using butanoic, hexanoic and decanoic acids on its capacity as a delivery vector. Hexanoyl octaarginine (C6R8-Alexa) showed the highest efficiency of cellular uptake of the studied variants, ten times higher than R8-Alexa. C6R8-Alexa also produced a diffuse cytosolic distribution. On the other hand, a less significant effect of C6R8 over R8 was observed for the delivery of proteins, suggesting that the advantage of C6R8 may be obtained during the delivery of relatively small molecular-weight compounds. Although less prominent than at 37 °C, a significant cytosolic distribution of C6R8-Alexa was observed at 4 °C, and this suggested the potential ability of the C6R8 peptide for direct penetration through plasma membranes.

© 2010 Elsevier B.V. All rights reserved.

1. Introduction

While plasma membranes play a crucial function to maintain cellular structures and functions, they work as a strong barrier against the intracellular delivery of membrane-impermeable agents [1]. Arginine-rich cell-penetrating peptides (CPPs), such as HIV-1 TAT and octaarginine (R8), have been employed as a delivery vector of these agents into cells [2–5]. The contribution of endocytosis including macropinocytosis, a form of actin-driven and clathrin/caveola-independent endocytosis, has been reported for the cellular uptake of arginine-rich CPPs and their conjugates [6–10]. The cargo molecules taken up by the cells via endocytosis have to escape from endosomes to exert their biological activity in the cytosol and nucleus. One possible approach to improve the endosomal escape of the cargo molecules may be to introduce hydrophobic moieties onto peptides to increase their affinity to cell membranes (Fig. 1). Our previous study suggested that the increasing affinity of oligoarginines to a cell surface, e.g., increasing the number of arginines and removing serum proteins from the medium, would produce a change in the peptide uptake with a prominent cytosolic peptide distribution [11]. In addition, it has been demonstrated that an efficient intracellular delivery of genes and siRNA was achieved by the non-covalent complex formation of these molecules with stearyl and cholesteryl oligoarginines [12–14]. Improvement of efficiency in CPP-mediated delivery by lipidation has also been reported [15–17]. However, only limited information is available about the intracellular fate of the acylated oligoarginines and their applicability as a delivery vector for peptides/proteins as well as compounds of relatively small molecular weight.

In this study, using octaarginine (R8) peptides as a typical arginine-rich CPP, the effect of N-terminal acylation on cellular uptake was evaluated using fatty acids having various chain lengths (Table 1). The study using the Alexa488 labeled acylated CPPs showed that hexanolyl R8 (C6R8-Alexa) produced ten times greater cellular uptake by the HeLa cells with efficient spread of the peptide signals in the cytosol and nucleus. The internalization mechanisms, and scope and limitation of the peptide as a delivery vector were also discussed.

2. Results and discussion

2.1. Effect of acylation on cellular uptake of octaarginine

We first examined the effect of the fatty acid modification of octaarginine (R8) in terms of the total cellular uptake and cellular distribution. R8 modified with straight-chain fatty acids of different chain lengths, namely, butanoyl R8 (C4R8), hexanoyl R8 (C6R8), decanoyl R8 (C10R8), tetradecanoyl (myristoyl) R8 (C14R8), and octadecanoyl (stearyl) R8 (C18R8) were prepared by Fmoc-solid-

Abbreviations: R8, Octaarginine; C6R8, Hexanoyl octaarginine; FACS, Fluorescence-activated cell sorter; CLSM, Confocal laser scanning microscopy; PI, Propidium iodide; CytD, Cytochalasin D; Ub, Ubiquitin; CA, Carbonic anhydrase; EMCS, *N*-(6-malaimidocaproyloxy) succinimide; PAD, Proapoptotic domain peptide; α-MEM, α-minimum essential medium; RP-HPLC, Reverse phase high-performance liquid chromatography; MALDI-TOFMS, Matrix-assisted laser desorption ionization-time-of-flight mass spectrometry.

* Corresponding author. Tel.: +81 774 38 3210; fax: +81 774 32 3038.
E-mail address: futaki@scl.kyoto-u.ac.jp (S. Futaki).

0168-3659/$ – see front matter © 2010 Elsevier B.V. All rights reserved.
doi:10.1016/j.jconrel.2010.02.004

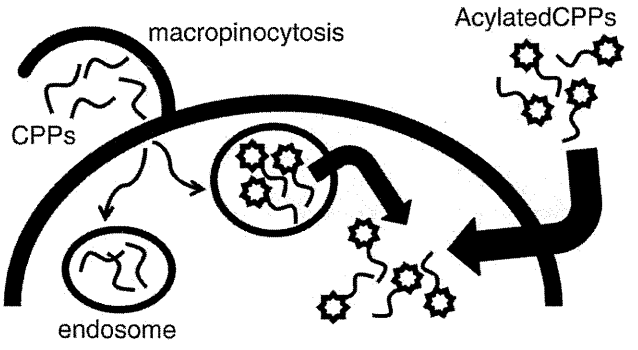

Fig. 1. Possible internalization routes of acylated CPPs. Acylation of arginine-rich CPPs may increase the interaction of the peptides with the membrane to facilitate the endosomal escape after their endocytic uptake or to promote direct penetration through the plasma membranes.

Table 1
Structures of the peptides used in this study.

Name	Fatty acid	Structure
R8	–	RRRRRRRRGC-amide
C4R8	Butanoic acid	C_3H_7CO-RRRRRRRRGC-amide
C6R8	Hexanoic acid	$C_5H_{11}CO$-RRRRRRRRGC-amide
C10R8	Decanoic acid	$C_9H_{19}CO$-RRRRRRRRGC-amide

phase peptide synthesis, and labeled with Alexa488 [CnR8-Alexa ($n=4$, 6, 10, 14, and 18, respectively)]. Alexa488 modification was conducted to assess peptide internalization by CLSM observation and FACS analysis. This fluorophore can also be regarded as a model of a small molecular-weight compound to be delivered into cells with the help of the peptide vector.

For CLSM analysis, HeLa cells were treated with 10 μM peptides at 37 °C for 30 min in α-minimum essential medium containing 10% serum [α-MEM(+)]. The cells treated with Alexa488-labeled R8 (R8-Alexa) showed punctate signals (Fig. 2A). This suggested that the fluorophore was taken up by the cells together with R8 via endocytosis and that the majority of the fluorophore was trapped in the endosomes without translocating into the cytosol as previously reported [7]. The C4R8-Alexa also yielded similar punctate signals in the cells. In contrast, C6R8-Alexa and C10R8-Alexa yielded diffuse signals throughout the cells together with punctate endosome-like signals. This suggested that the fluorophore was efficiently delivered into the cytosol and nucleus by conjugation with these peptides. Note that all the CLSM images in this study were obtained using live cells and the diffuse signals were not due to artifacts by fixation as previously pointed out [6]. Therefore, N-terminus acylation with hexanoic and decanoic acids effectively facilitated the translocation of R8-Alexa into the cytosol. Further elongation of the acyl chain lowered the solubility of the peptides, and it was difficult to treat the cells with C14R8-Alexa and C18R8-Alexa due to the formation of insoluble aggregates when applied to the culture media, thus no further study on their cellular uptake was conducted (data not shown).

FACS analysis of the cells treated with these conjugates showed that the use of C6R8 yielded the highest amount of total cellular uptake of the fluorophore (i.e., the sum of the fluorophore trapped in the endosomes and delivered into the cytosol). More than a 13-time

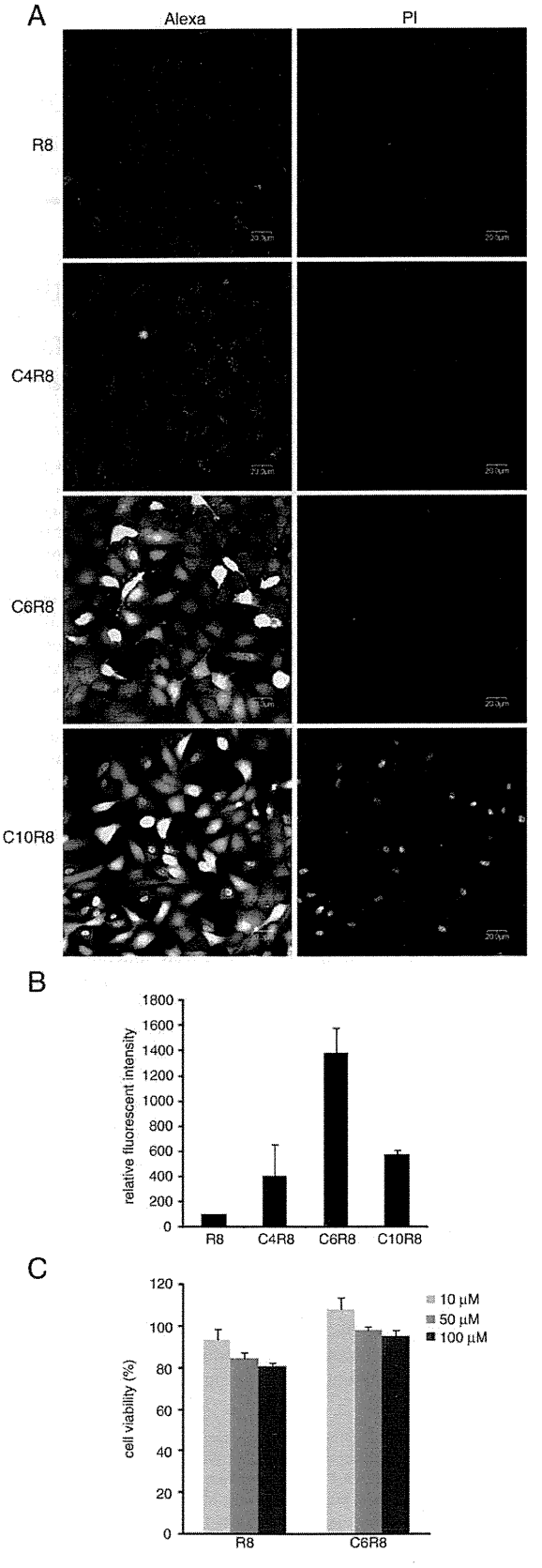

Fig. 2. CLSM analysis of the cells treated with acylated R8 peptides. (A) The HeLa cells were incubated with acylated R8 peptides labeled with Alexa488 (10 μM) in the presence of 5 μM propidium iodide (PI) for 30 min at 37 °C in α-MEM containing 10% serum [α-MEM(+)] prior to the CLSM analysis. Scale bar, 20 μm. (B) FACS analysis of the total cellular uptake of the acylated R8 peptides. The cells were treated with 10 μM peptides for 30 min at 37 °C in α-MEM(+) and the total cellular uptake was quantified. (C) Cytotoxicity analysis using the WST-1 assay. The HeLa cells were treated with non-labeled C6R8 or R8 for 24 h.

higher amount of the fluorophore was delivered into the cells using C6R8 than when using R8 as a vector (Fig. 2B). C10R8 produced an uptake of about 40% as much as that of C6R8. Although C4R8 produced endosome-like punctate signals of the fluorophore as in the case of R8, the total cellular uptake was about four times as much as the latter.

Enhanced cellular uptake of the fluorophore conjugated with acylated R8 may be attributed to the increased interaction between the peptides and membranes. On the other hand, the increasing membrane interaction or amphiphilicity of the peptide vectors may enhance membrane perturbation. This was assessed by coincubation of the acylated peptide vectors with a membrane-impermeable nuclear staining dye, propidium iodide (PI) (Fig. 2A, right panels). Perturbation of the plasma membranes would allow the dye to penetrate through the membranes resulting in nuclear staining. No significant nuclear staining was observed for the cells treated with 10 μM R8-, C4R8-, and C6R8-Alexa conjugates, suggesting very little effect of these vectors on the integrity of the plasma membranes under the given conditions. However, a considerable number of cells treated with C10R8-Alexa were PI positive. Excessive increase in the acyl chain length of the vectors would accompany the change in the surfactant effect of the vectors and thus produce a perturbation of the plasma membranes.

These results suggested the potential superiority of C6R8 over R8 as an intracellular delivery vector of compounds of relatively small molecular weight. The absence of a significant cytotoxicity of the C6R8 was further confirmed. To avoid the possible toxicity caused by the Alexa488 moiety, HeLa cells were treated with C6R8 without Alexa labeling ($C_5H_{11}CO$-R8-amide), and viability after treatment with C6R8 for 24 hr was analyzed using the WST-1 assay (Fig. 2C). Even in the case when the cells were treated with 100 μM C6R8, cell viability was higher than 90% as compared to the control cells and this was comparable or lower than that of R8. Therefore, modification with hexanoic acid endowed no significant cytotoxicity to R8.

2.2. Internalization methods of C6R8-Alexa

The involvement of endocytosis for the cellular uptake of arginine-rich CPPs has been reported and macropinocytosis is now regarded as one of the major endocytic uptake pathways of these peptides and their conjugates [7,8]. Macropinocytosis is clathrin-independent and actin-driven endocytosis. We have recently demonstrated that the interaction of oligoarginine with membrane-associated proteoglycans induces actin rearrangement and the eventual macropinocytotic uptake of the peptides [10]. To analyze the contribution of macropinocytosis to the cellular uptake of C6R8 as in the case of R8, HeLa cells were treated with 10 μM R8-Alexa or C6R8-Alexa in the presence and absence of 5 μM cytochalasin D (CytD) in α-MEM(+) for 10 min prior to the CLSM observation (Fig. 3A).

In the absence of CytD, C6R8-Alexa yielded significant diffuse signals in the cytosol. There was a range of intensity of the endosome-like C6R8-Alexa signals observed in the cells; some cells yielded intense punctate signals in the perinuclear area together with diffuse cytosolic signals (shown with an arrow) whereas more accumulated signals to the nuclei were observed in other cells (a triangle). On the other hand, R8 yielded only punctate signals and this further confirmed the acceleration effect of the hexanoyl moiety on the translocation of R8-Alexa into the cytosol.

CytD treatment of the cells would lead to F-actin depolymerization and the eventual inhibition of the macropinocytic uptake [18]. Similar to the case of R8-Alexa, a significant decrease in the endosome-like punctate signals of C6R8-Alexa was observed in the CytD-treated cells (Fig. 3A). FACS analysis of the CytD-treated cells showed a 30–40% decrease in the total cellular uptake (Fig. 3B). This suggested the possible involvement of the actin-driven pathways including macropinocytosis in the cellular uptake of C6R8-Alexa. On the other hand, diffuse signals of C6R8-Alexa in the presence of CytD also suggested the contribution of cellular uptake other than the actin-driven pathways.

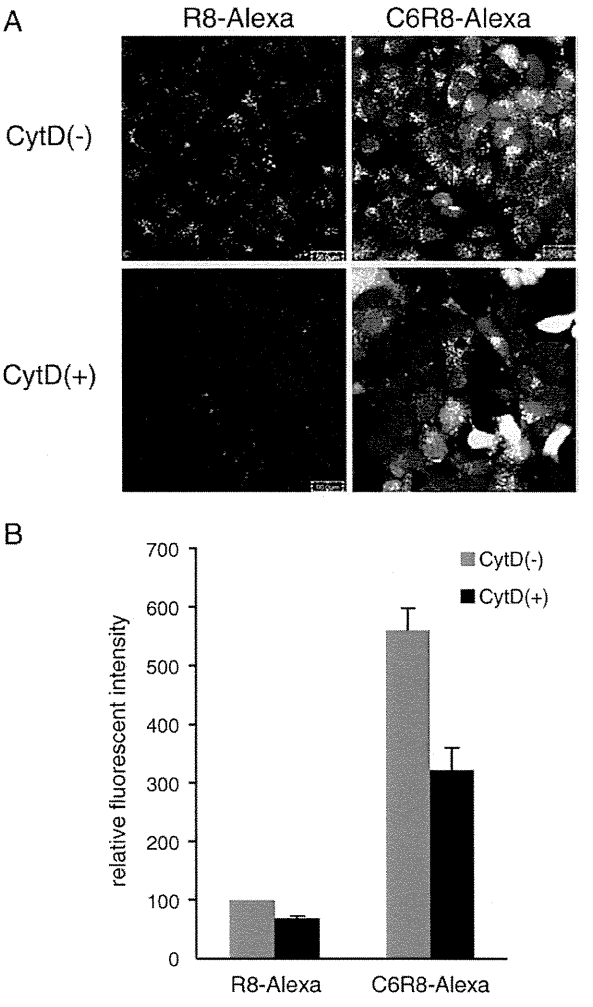

Fig. 3. Effect of cytochalasin D (CytD) on the cellular uptake of C6R8-Alexa. (A) The HeLa cells were incubated with 10 μM C6R8-Alexa or R8-Alexa in the absence and presence of 5 μM CytD for 10 min at 37 °C in α-MEM(+) and distribution of the peptide was analyzed by CLSM. Scale bar, 50 μm. (B) FACS analysis of C6R8-Alexa or R8-Alexa taken up by the cells in 10 min at 37 °C in the absence and presence of 5 μM CytD.

Endocytosis is an energy dependent pathway and is usually suppressed when the cells are treated at 4 °C [19,20]. To assess the involvement of non-endocytic pathways for the internalization of C6R8-Alexa, HeLa cells were incubated with 10 μM R8-Alexa or C6R8-Alexa in α-MEM(+) for 30 min at 37 °C and 4 °C (Fig. 4A). Endosome-like punctate signals were predominantly observed for the cells treated with R8-Alexa at 37 °C and diffuse signals spreading over all the cells together with endosome-like punctate signals for the C6R8-Alexa treated cells (Fig. 4A, upper panels). A significant decrease in the fluorescent intensity was observed when the cells were treated with R8-Alexa or C6R8-Alexa at 4 °C (Fig. 4A, lower panels). However, C6R8-Alexa still yielded significant diffuse signals in the cytosol and nucleus even after this 4 °C-treatment, accompanied by no punctate, endosome-like signals. A similar observation was obtained for the R8-Alexa treated cells at 4 °C, while accompanied by much less intense signals as in the case of the C6R8-Alexa treated cells. These results suggested the possibility that both R8-Alexa and C6R8-Alexa were internalized into cells at 4 °C, presumably by a non-endocytic route and through direct penetration throughout the plasma membranes as reported, [11,19,20]. C6R8-Alexa having an additional hydrophobic affinity to plasma membranes showed a greater extent of translocation through the membranes. It would be interesting to determine why diffuse labeling was only observed for cells treated with these

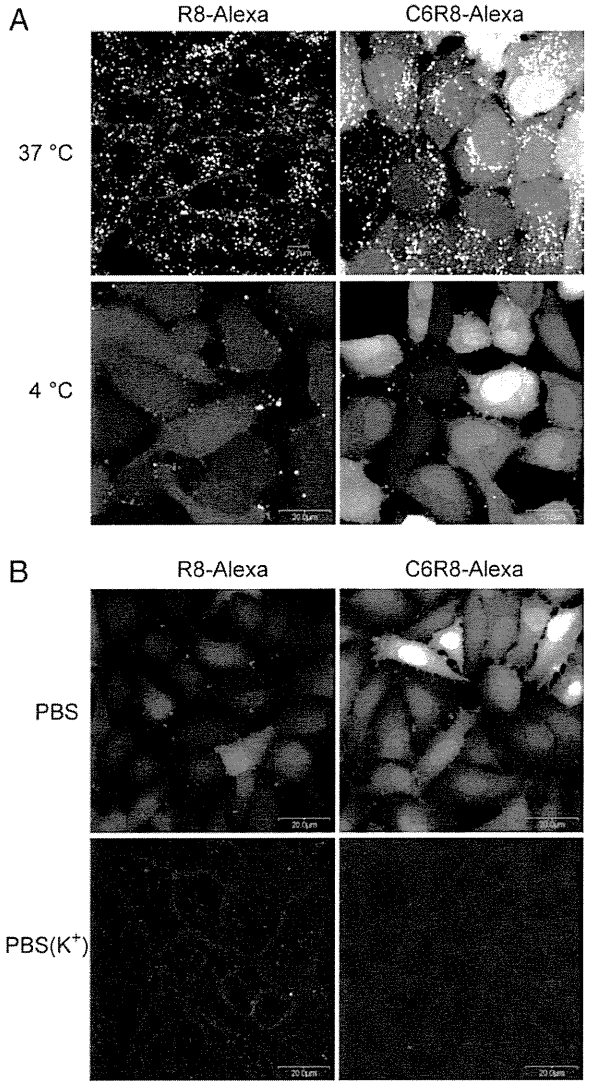

Fig. 4. Effect of low temperature treatment and cancellation of membrane potential on the internalization of C6R8 and R8. (A) The HeLa cells were incubated with 10 μM C6R8-Alexa or R8-Alexa for 30 min at 4 °C or 37 °C in α-MEM(+) and the cellular localization of the peptides was analyzed by CLSM. (B) The HeLa cells were incubated with 5 μM C6R8-Alexa or R8-Alexa for 10 min at 37 °C in PBS(K^+) or PBS. 5 μM peptides were employed to avoid saturation of the fluorescent signals in the CLMS analysis since C6R8-Alexa internalizes into cells more efficiently in PBS than in the α-MEM(+). Scale bar, 20 μm.

peptides at 4 °C. It has been reported that cell-surface accumulation of arginine-rich CPPs at a concentration exceeding a certain threshold leads to direct and energy-independent translocation of the peptides [11,20,21]. Inhibition of endocytic uptake of these peptides at 4 °C would therefore contribute to increase the peptide concentration on plasma membranes and thus promote diffuse cytosolic labeling.

The membrane potential has been suggested as one of the critical factors for cellular uptake of the arginine-rich CPPs [22,23]. We examined whether the translocation of C6R8 is dependent on the membrane potential. Cells were incubated with 5 μM R8-Alexa and C6R8-Alexa for 10 min in PBS(K^+), where Na^+ in the phosphate buffered saline (PBS) is replaced with an equimolar amount of K^+, and this leads to cancellation of the membrane potentials [22]. A drastic decrease in the intracellular fluorescent signals was observed in the CLSM analysis for the cells treated with both R8-Alexa and C6R8-Alexa in PBS(K^+) (Fig. 4B), and this suggested that the membrane potential also plays a crucial role in the translocation of the C6R8-Alexa as in the case of R8-Alexa. Treatment of the cells with R8-Alexa and C6R8-Alexa in PBS (Fig. 4B, upper panels) yielded more diffuse cytosolic labeling than in experiments where the peptide was incubated in α-MEM(+) (Fig. 4A, upper panels). Adsorption of arginine-rich CPPs to serum proteins would reduce cell-surface concentration of the peptides together with cytosolic signals of the peptides as reported previously [11].

2.3. Applicability of C6R8 as a protein/peptide delivery vector

The above results suggested the advantage of C6R8 as an intracellular delivery vector to the R8. Since the effects of cargo molecules on the efficacy of intracellular delivery have been reported, [24,25] we next examined the effect of protein conjugation on the intracellular delivery using C6R8. Conjugates of the Alexa-labeled ubiquitin (9 kDa) with R8 and C6R8 were prepared using the heterobifunctional cross-linking agent EMCS [=*N*-(6-maleimidocaproyloxy)succinimide] (R8-Ub-Alexa and C6R8-Ub-Alexa, respectively) [26]. Treatment of the HeLa cells with 10 μM C6R8-Ub-Alexa at 37 °C for 30 min produced significant punctate signals in the cells (Fig. 5A). Diffuse signals of the conjugates in the cytosol were also observed for ~20% of the cells treated with C6R8-Ub-Alexa. In contrast, only punctate signals with a lower intensity were observed in the R8-Ub-Alexa treated cells. Conjugates of carbonic anhydrase (29 kDa) with these peptides were similarly prepared (R8-CA-Alexa and C6R8-CA-Alexa, respectively) and incubated with HeLa cells. Although C6R8-CA-Alexa produced more intense signals in the cells compared to R8-CA-Alexa, only punctate signals were observed in both cases (Fig. 5B). Therefore, the conjugation with C6R8 also effectively improved the cellular uptake of the proteins. However, as the molecular weight of the cargo molecules was higher, the acceleration effect of the cytosolic translocation seems to become less obvious.

The proapoptotic domain (PAD) peptide has an amphiphilic, cationic sequence of $_D$-$(KLAKLAK)_2$ and is by itself non-toxic to eukaryotic cells even at relatively high concentrations up to 300 μM [27]. However, PAD conjugated to CPPs inhibits cell proliferation in the low micromolar range by perturbation of the mitochondrial membrane and the induction of apoptotic cell death [7]. Here, the effect of the C6R8 conjugation on the efficacy during the intracellular delivery of PAD was assessed in comparison to that by R8 using human malignant glioma cells expressing the wild type p53 protein (A172) and mutant p53 protein (T98G). The PAD was connected with C6R8 or R8 by disulfide cross-linking (C6R8-ss-PAD and R8-ss-PAD, respectively) and treated with these glioma cells (5–20 μM for 24 h), and the viability of the cells was analyzed by the WST-1 assay (Fig. 6A, left). A marked decrease in viability was observed when the A172 cells were treated with C6R8-ss-PAD (10 and 20 μM). At 20 μM, viability of the C6R8-ss-PAD treated cells was less than 20% while that for the R8-ss-PAD treated cells was only 65%. Therefore, C6R8 effectively work as an intracellular delivery vector of the PAD peptide for A172 cells.

On the other hand, different results were obtained using the T98G cells. The treatment of T98G cells with 20 μM C6R8-ss-PAD produced only about a 40% cell death and there was no significant superiority of C6R8 over R8 in this case (Fig. 6A, right). We hypothesized that this would be due to the efficiency in cellular uptake or distribution into the cytosol of the C6R8. Therefore, we examined the total cellular uptake of C6R8-Alexa and R8-Alexa by FACS analysis and CLSM observations in both cells. However, this yielded no significant differences in the cellular uptake of C6R8-Alexa to R8-Alexa between these cells (data not shown). A CLSM analysis of the C6R8-Alexa treated cells showed diffuse cytosolic signals but only punctate signals were obtained for the R8-Alexa treated cells (Fig. 6B). There is currently no distinct explanation at current stage about the

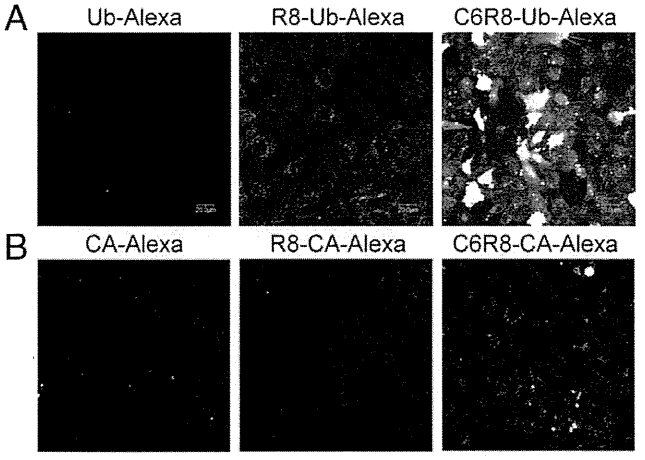

Fig. 5. Intracellular delivery of ubiquitin (Ub) and carbonic anhydrase (CA) using C6R8 and R8. (A) The HeLa cells were treated with C6R8-Ub-Alexa or R8-Ub-Alexa (10 μM) at 37 °C for 30 min in α-MEM(+) prior to the CLSM analysis. Scale bar, 20 μm. (B) The HeLa cells were similarly treated with C6R8-CA-Alexa or R8-CA-Alexa (10 μM) at 37 °C for 30 min.

inconsistency between the extent of cellular uptake (or cytosolic diffusion) and bioactivity of these peptides in T98G cells; the diminished p53 activity of the mutant p53 expressed in the T98G cells may be one possible reason because often it leads to cells with resistance against anti-cancer reagents [28].

3. Conclusion

The results obtained in this study suggest the potential of fatty acid modification of arginine-rich CPPs to improve efficacy in intracellular delivery. We employed R8 as a typical arginine-rich CPP, and the modification with hexanoic acid was shown to produce a considerable improvement in the cellular uptake and cytosolic distribution of the cargo molecules with no significant cytotoxicity. Of note is that all the experiments in this study were conducted using serum-containing medium, and this suggests the potential expandability of this approach for in vivo applications.

C6R8 shares the similarity of internalization methods with R8, including the involvement of macropinocytosis or other actin-driven endocytosis, possible direct translocation into cytosol at 4 °C and contribution of membrane potentials to internalization. Internalization of these peptide vectors and their conjugates with cargos would be accomplished based on a balance of these factors. Lack of a notable cytotoxicity by the C6R8 treatment suggested that the translocation was not accomplished via a simple pore formation or perturbation on the membranes. Detailed analyses of the internalization methods of these peptides referring to the differences in the hydrophobicity may provide novel insights into the modes of peptide–membrane interaction.

Increment of membrane interaction by hexanoic acid modification led to a higher extent of cytosolic distribution of C6R8 as compared to R8. Acylation of R8 with decanoic or the longer-chain fatty acids produced a higher cytotoxicity and accompanied the aggregate formation. Therefore, there must be a range of hydrophobicity to accomplish the optimum cytosolic delivery. Recently, we reported that the addition of a hydrophobic peptide segment [FFLIPKG, designated as penetration accelerating sequence (Pas)] to arginine-rich CPPs also facilitated the cytosolic distribution of the cargo molecules [29]. Therefore, adding the hydrophobic cores to arginine-rich CPPs could be a way to improve their efficiency of the cytosolic delivery. On the other hand, we also found that there can be a certain differences in the internalization efficiency among the peptides with a similar hydrophobicity [e.g., Pas modified R8 (FFLIPKG-RRRRRRRR) and the retro peptide RRRRRRRR-GKPILFF] and it should be noted that there must be other additional factors that determine the methods of internalization of these peptides.

When the C6R8 was conjugated with ubiquitin (9 kDa), C6R8-Ub-Alexa showed a significantly higher cellular uptake and cytosolic distribution into the cytosol than R8-Ub-Alexa. However, for the delivery of carbonic anhydrase (28 kDa), the effect of acylation became smaller, presumably due to larger molecular size of the carbonic anhydrase that prevents penetration through the membranes. Although further evaluation is necessary, this study has provided important information on the design of peptide-based intracellular delivery vectors.

4. Experimental procedures

4.1. Peptides

For the preparation of the N-terminus acylated peptides, the peptide chain was constructed using Fmoc (9-fluorenylmethyloxycarbonyl) solid-phase peptide synthesis, and the N-terminus of the peptide resin was acylated using the corresponding fatty acid with diisopropylcarbodiimide in the presence of N-hydroxybenzotriazole as coupling agents as previously reported [12]. Treatment of the acylated peptide resin with trifluoroacetic acid in the presence of 5% ethanedithiol followed by reverse phase high-performance liquid chromatography (RP-HPLC) produced the desired peptides. For Alexa labeling, the HPLC purified CnR8GC peptides ($n=4$, 6, 10, 14, and 18) were treated with the Alexa Fluor 488 C_5 maleimide sodium salt (Invitrogen) as previously reported [10]. Actual sequences of the peptides follows: C6R8, C_5H_{11}CO-RRRRRRRR-amide; CnR8GC, C_mH_{2m+1}CO-RRRRRRRRGC-amide ($n=4$, 6, 10, 14, and 18; $m=n-1$); CnR8-Alexa, C_mH_{2m+1}CO-RRRRRRRRGC(Alexa488)-amide ($n=4$, 6, 10, 14, and 18; $m=n-1$); R8, RRRRRRRR-amide; R8GC, RRRRRRRRGC-amide; and R8-Alexa, RRRRRRRRGC(Alexa488)-amide.

The C6R8-ss-PAD was prepared via selective disulfide cross-linking between C6R8GC and the CG-$_D$-$(KLAKLAK)_2$-amide by activation of the cysteine in the CG-$_D$-$(KLAKLAK)_2$-amide via pyridine sulfenylation [7]. For the preparation of R8-ss-PAD, R8GC was employed instead of C6R8GC.

The purity and structures of the peptides used in this study were confirmed by HPLC and matrix-assisted laser desorption ionization-time-of-flight mass spectrometry (MALDI-TOFMS), respectively.

4.2. Conjugates of ubiquitin with R8 and C6R8

Alexa 488-labeling of ubiquitin was conducted by the treatment of ubiquitin with Alexa 488 carboxylic acid, succinimidyl ester (Invitrogen) (3 eq) followed by cross-linking with R8GC or C6R8GC using *N*-(6-maleimidocaproyloxy)succinimide (EMCS) (Dojindo) [3 eq each to Alexa-labeled ubiquitin] as reported [26]. After the reactions, the excess reagents or peptides were removed by ultrafiltration using a Microcon YM-10 centrifuging filter (Millipore) (molecular weight cut off = 10,000) at 14,000×*g* for 24 min. Ubiquitin was obtained from Sigma. Conjugates of carbonic anhydrase (Sigma) with R8GC or C6R8GC were similarly prepared (MicroconYM-30 was used for ultrafiltration). The concentration of these conjugates was described in this report on the basis of the absorbance of fluorophore.

4.3. Cell culture

Human cervical cancer-derived HeLa cells were cultured on 100 mm dishes in α-minimum essential medium supplemented with 10% (v/v) fetal bovine serum (GIBCO) [α-MEM(+)]. Human glioblastoma-derived cells including A172 (wild type) and T98G (variant) were cultured in D-MEM (Dulbecco's Modified Eagle Medium) supplemented with 10% (v/v) fetal bovine serum (GIBCO).

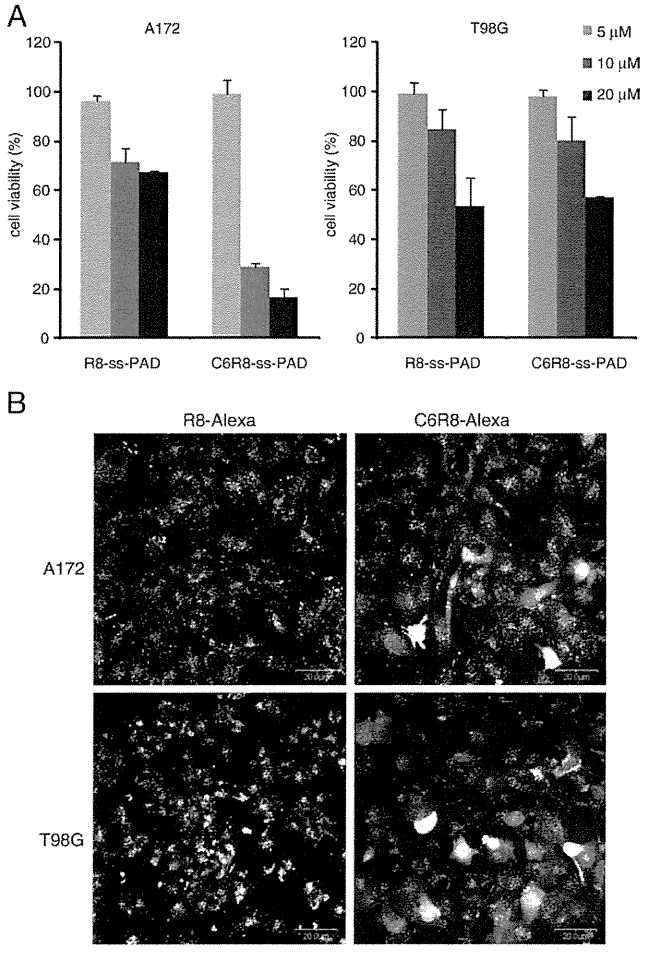

Fig. 6. Assessment of internalization efficiency in terms of bioactivity exerted by the intracellularly delivered PAD peptide. (A) C6R8-ss-PAD and R8-ss-PAD were incubated with A172 and T98G cells for 24 h and the cell viability was analyzed by the WST-1 assay. (B) The CLSM analysis of the A172 and T98G cells treated with C6R8-Alexa and R8-Alexa (10 μM) for 30 min.

Cells were maintained at 37 °C in a humidified 5% CO_2 incubator, and a subculture was performed every 3–4 days.

4.4. Confocal microscopy

HeLa cells (1.5×10^5 cells/well) were plated in 35 mm glass-bottomed dishes (Iwaki) and cultured for 48 h. The cells were washed twice with serum-free medium prior to incubation with the peptides or proteins in 200 μL of α-MEM containing 10% (v/v) fetal bovine serum [α-MEM (+)]. After incubation for 30 min, the incubated medium was removed and the cells were washed twice with cold serum-free medium. The intracellular distribution was immediately analyzed without fixing using a confocal laser scanning microscope (Olympus FV300) equipped with a ×40 objective. For experiments using cytocharasin D (CytD), the cells were preincubated with 5 μM CytD in α-MEM (+) for 30 min prior to incubation with the peptide and CytD in α-MEM (+) for 10 min. For the 4 °C experiments, cells were preincubated in a refrigerator (4 °C) for 1 h. Washing and incubation of the cells were then conducted using cold medium and the 4 °C refrigerator, respectively, prior to observation of the cells. For experiments investigating the contribution of the membrane potential, a buffer PBS(K^+) in which the sodium salts in PBS(−) were replaced with equimolar amounts of the equivalent potassium salts was used.

4.5. Flow cytometry

HeLa cells (4×10^4 cells/well) were plated in 24 well microplates (Iwaki) and cultured for 48 h. The cells were washed twice with serum-free medium prior to incubation with peptides (10 μM) in α-MEM (+). The cells were then washed twice with PBS containing 0.5 mg/mL heparin to ensure the removal of cell-surface adsorbed peptides and incubated with 0.01% trypsin in PBS for 10 min at 37 °C. The cells were harvested and centrifuged at 3000 rpm for 5 min. The cell pellet was then suspended with PBS containing 0.5 mg/mL heparin followed by centrifuging. After an additional two washes with PBS and centrifuging, the cells were suspended in 400 μL of PBS and filtered for fluorescence analysis by a FACS Calibur flow cytometer (BD Biosciences) using a 488 nm laser excitation and a 515–545 nm emission filter. Each sample was analyzed for 10,000 events.

4.6. WST-1 assay

HeLa, A172, and T98G cells (5×10^3 cells/well) were plated in 96 well microplates (Iwaki) and cultured for 48 h. After removing the medium, the cells were incubated with peptide-containing medium for 24 h at 37 °C and then a WST-1 assay were conducted following the procedures provided by the supplier (Roche).

Acknowledgments

This work was supported in part by Grants-in-Aid for Scientific Research from the Ministry of Education, Culture, Sports, Science and Technology of Japan. H. H. and K. T. are grateful for a JSPS Research Fellowship for Young Scientists.

References

[1] A. El-Sayed, S. Futaki, H. Harashima, Delivery of macromolecules using arginine-rich cell-penetrating peptides: ways to overcome endosomal entrapment, AAPS J. 11 (2009) 13–22.
[2] S. Futaki, Oligoarginine vectors for intracellular delivery: design and cellular-uptake mechanisms, Biopolymers 84 (2006) 241–249.
[3] J.S. Wadia, S.F. Dowdy, Transmembrane delivery of protein and peptide drugs by TAT-mediated transduction in the treatment of cancer, Adv. Drug Deliv. Rev. 57 (2005) 579–596.
[4] E.A. Goun, T.H. Pillow, L.R. Jones, J.B. Rothbard, P.A. Wender, Molecular transporters: synthesis of oligoguanidinium transporters and their application to drug delivery and real-time imaging, Chembiochemistry 7 (2006) 1497–1515.
[5] S. Futaki, T. Suzuki, W. Ohashi, T. Yagami, S. Tanaka, K. Ueda, Y. Sugiura, Arginine-rich peptides. An abundant source of membrane-permeable peptides having potential as carriers for intracellular protein delivery, J. Biol. Chem. 276 (2001) 5836–5840.
[6] J.P. Richard, K. Melikov, E. Vives, C. Ramos, B. Verbeure, M.J. Gait, L.V. Chernomordik, B. Lebleu, Cell-penetrating peptides. A reevaluation of the mechanism of cellular uptake, J. Biol. Chem. 278 (2003) 585–590.
[7] I. Nakase, M. Niwa, T. Takeuchi, K. Sonomura, N. Kawabata, Y. Koike, M. Takehashi, S. Tanaka, K. Ueda, J.C. Simpson, A.T. Jones, Y. Sugiura, S. Futaki, Cellular uptake of arginine-rich peptides: roles for macropinocytosis and actin rearrangement, Mol. Ther. 10 (2004) 1011–1022.
[8] J.S. Wadia, R.V. Stan, S.F. Dowdy, Transducible TAT-HA fusogenic peptide enhances escape of TAT-fusion proteins after lipid raft macropinocytosis, Nat. Med. 10 (2004) 310–315.
[9] I. Nakase, T. Takeuchi, G. Tanaka, S. Futaki, Methodological and cellular aspects that govern the internalization mechanisms of arginine-rich cell-penetrating peptides, Adv. Drug Deliv. Rev. 60 (2008) 598–607.
[10] I. Nakase, A. Tadokoro, N. Kawabata, T. Takeuchi, H. Katoh, K. Hiramoto, M. Negishi, M. Nomizu, Y. Sugiura, S. Futaki, Interaction of arginine-rich peptides with membrane-associated proteoglycans is crucial for induction of actin organization and macropinocytosis, Biochemistry 46 (2007) 492–501.
[11] M. Kosuge, T. Takeuchi, I. Nakase, A.T. Jones, S. Futaki, Cellular internalization and distribution of arginine-rich peptides as a function of extracellular peptide concentration, serum, and plasma membrane associated proteoglycans, Bioconjug. Chem. 19 (2008) 656–664.
[12] S. Futaki, W. Ohashi, T. Suzuki, M. Niwa, S. Tanaka, K. Ueda, H. Harashima, Y. Sugiura, Stearylated arginine-rich peptides: a new class of transfection systems, Bioconjug. Chem. 12 (2001) 1005–1011.

[13] L. Tönges, P. Lingor, R. Egle, G.P. Dietz, A. Fahr, M. Bähr, Stearylated octaarginine and artificial virus-like particles for transfection of siRNA into primary rat neurons, RNA 12 (2006) 1431–1438.
[14] W.J. Kim, L.V. Christensen, S. Jo, J.W. Yockman, J.H. Jeong, Y.H. Kim, S.W. Kim, Cholesteryl oligoarginine delivering vascular endothelial growth factor siRNA effectively inhibits tumor growth in colon adenocarcinoma, Mol. Ther. 14 (2006) 343–350.
[15] U. Koppelhus, T. Shiraishi, V. Zachar, S. Pankratova, P.E. Nielsen, Improved cellular activity of antisense peptide nucleic acids by conjugation to a cationic peptide-lipid (CatLip) domain, Bioconjug. Chem. 19 (2008) 1526–1534.
[16] A.R. Nelson, L. Borland, N.L. Allbritton, C.E. Sims, Myristoyl-based transport of peptides into living cells, Biochemistry 46 (2007) 14771–14781.
[17] J. Fernandez-Carneado, M.J. Kogan, N. Van Mau, S. Pujals, C. Lopez-Iglesias, F. Heitz, E. Giralt, Fatty acyl moieties: improving Pro-rich peptide uptake inside HeLa cells, J. Pept. Res. 65 (2005) 580–590.
[18] P. Sampath, T.D. Pollard, Effects of cytochalasin, phalloidin, and pH on the elongation of actin filaments, Biochemistry 30 (1991) 1973–1980.
[19] M.M. Fretz, N.A. Penning, S. Al-Taei, S. Futaki, T. Takeuchi, I. Nakase, G. Storm, A.T. Jones, Temperature-, concentration- and cholesterol-dependent translocation of L- and D-octa-arginine across the plasma and nuclear membrane of $CD34^+$ leukaemia cells, Biochem. J. 403 (2007) 335–342.
[20] C.L. Watkins, D. Schmaljohann, S. Futaki, A.T. Jones, Low concentration thresholds of plasma membranes for rapid energy-independent translocation of a cell-penetrating peptide, Biochem. J. 420 (2009) 179–189.
[21] F. Duchardt, M. Fotin-Mleczek, H. Schwarz, R. Fischer, R. Brock, A comprehensive model for the cellular uptake of cationic cell-penetrating peptides, Traffic 8 (2007) 848–866.
[22] J.B. Rothbard, T.C. Jessop, R.S. Lewis, B.A. Murray, P.A. Wender, Role of membrane potential and hydrogen bonding in the mechanism of translocation of guanidinium-rich peptides into cells, J. Am. Chem. Soc. 126 (2004) 9506–9507.
[23] T. Takeuchi, M. Kosuge, A. Tadokoro, Y. Sugiura, M. Nishi, M. Kawata, N. Sakai, S. Matile, S. Futaki, Direct and rapid cytosolic delivery using cell-penetrating peptides mediated by pyrenebutyrate, ACS Chem. Biol. 1 (2006) 299–303.
[24] J.R. Maiolo, M. Ferrer, E.A. Ottinger, Effects of cargo molecules on the cellular uptake of arginine-rich cell-penetrating peptides, Biochim. Biophys. Acta 1712 (2005) 161–172.
[25] G. Tünnemann, R.M. Martin, S. Haupt, C. Patsch, F. Edenhofer, M.C. Cardoso, Cargo-dependent mode of uptake and bioavailability of TAT-containing proteins and peptides in living cells, FASEB J. 20 (2006) 1775–1784.
[26] K. Takayama, A. Tadokoro, S. Pujals, I. Nakase, E. Giralt, S. Futaki, Novel system to achieve one-pot modification of cargo molecules with oligoarginine vectors for intracellular delivery, Bioconjug. Chem. 20 (2009) 249–257.
[27] H.M. Ellerby, W. Arap, L.M. Ellerby, R. Kain, R. Andrusiak, G.D. Rio, S. Krajewski, C.R. Lombardo, R. Rao, E. Ruoslahti, D.E. Bredesen, R. Pasqualini, Anti-cancer activity of targeted pro-apoptotic peptides, Nat. Med. 5 (1999) 1032–1038.
[28] S. Fan, W.S. El-Deiry, I. Bae, J. Freeman, D. Jondle, K. Bhatia, A.J. Fornace Jr., I. Magrath, K.W. Kohn, P.M. O'Connor, p53 gene mutations are associated with decreased sensitivity of human lymphoma cells to DNA damaging agents, Cancer Res. 54 (1994) 5824–5830.
[29] K. Takayama, I. Nakase, H. Michiue, T. Takeuchi, K. Tomizawa, H. Matsui, S. Futaki, Enhanced intracellular delivery using arginine-rich peptides by the addition of penetration accelerating sequences (Pas), J. Control. Release 138 (2009) 128–133.

Journal of Controlled Release 149 (2011) 58–64

Contents lists available at ScienceDirect

Journal of Controlled Release

journal homepage: www.elsevier.com/locate/jconrel

Reprint of: Nanoparticles for ex vivo siRNA delivery to dendritic cells for cancer vaccines: Programmed endosomal escape and dissociation☆,☆☆

Hidetaka Akita [a], Kentaro Kogure [a,1], Rumiko Moriguchi [a], Yoshio Nakamura [a], Tomoko Higashi [a], Takashi Nakamura [a], Satoshi Serada [b], Minoru Fujimoto [b], Tetsuji Naka [b], Shiroh Futaki [c], Hideyoshi Harashima [a,*]

[a] Faculty of Pharmaceutical Sciences, Hokkaido University, Kita-12, Nishi-6, Kita-ku, Sapporo, Hokkaido 060-0812, Japan
[b] Laboratory for Immune Signal, National Institute of Biomedical Innovation, 7-6-8 Saito-Asagi, Ibaraki, Osaka 567-0085, Japan
[c] Institute for Chemical Research, Kyoto University, Uji, Kyoto 611-0011, Japan

ARTICLE INFO

Article history:
Received 14 September 2009
Accepted 7 January 2010
Available online 9 September 2010

Keywords:
siRNA
Vaccination
Dendritic cells
SOCS1
Intracellular trafficking

ABSTRACT

We previously developed octaarginine (R8)-modified lipid envelope-type nanoparticles for siRNA delivery (R8-MEND). Herein, we report on their *ex vivo* siRNA delivery to primary mouse bone marrow-derived dendritic cells (BMDCs) for potential use as a cancer vaccine. Quantitative imaging analysis of the intracellular trafficking of siRNA revealed that the dissociation process, as well as the rate of endosomal escape limits the siRNA efficiency of the prototype R8-MEND, prepared by the hydration method (R8-MEND$_{hydo}$). Successful endosomal escape was achieved by using a pH-dependent fusogenic peptide (GALA) modified on a lipid mixture that was optimized for endosomal fusion. Furthermore, a modified protocol for the preparation of nanoparticles, mixing the siRNA/STR-R8 complex and small unilamellar vesicles (R8/GALA-MEND$_{SUV}$), results in a more homogenous, smaller particle size, and results in a more efficient intracellular dissociation. Gene knockdown of the suppressor of cytokine signaling 1 (SOCS1), a negative-feedback regulator of the immune response in BMDCs resulted in an enhanced phosphorylation of STAT1, and the production of proinflammatory cytokines. Moreover, SOCS1-silenced BMDCs were more potent in suppressing tumor growth. Collectively, these results show that siRNA loaded in R8/GALA-MEND$_{SUV}$ efficiently suppresses endogenous gene expression and consequently enhances dendritic cell-based vaccine potency *in vivo*.

© 2010 Elsevier B.V. All rights reserved.

1. Introduction

RNA interference (RNAi) was discovered [1,2], in the latter part of the 20th century. This discovery represents a promising technique for use in the functional analysis of endogenous genes, and for curing intractable genetic diseases by the sequence-specific cleavage of mRNA [3–5]. One of the highly potential applications for the clinical use of siRNA is cancer vaccination. The suppressor of cytokine signaling 1 (SOCS1) is a negative-feedback regulator of immune cell responses to cytokines. Its expression is induced by cytokine-mediated stimulation, and is responsible for the negative-feedback of immunoresponse by blocking Janus kinase (JAK)-signal transducers, and activators of transcription (STAT) signaling pathways [6]. The suppression of SOCS1 gene expression in dendritic cells using a lentiviral vector has been shown to enhance their immunostimulatory capacity and to result in an enhanced antiviral and antitumor response [7,8]. However, the use of a viral vector may have unexpected, and serious adverse effects such as excessive inflammation [9] and oncogenicity due to the random insertion of viral genomic DNA into chromosomal DNA [10]. Therefore, non-viral delivery vehicles, which satisfy requirements for both high efficiency and safety, are essential for the realization of clinical applications of siRNA [11]. To be recognized by a RNA-induced silencing complex (RISC), siRNA must be delivered to the cytoplasm via invasion of the membrane. Therefore, novel nanotechnology is essential if various functional devices are integrated into one nano carrier for achieving both active cellular entry and endosomal escape. For an in vivo application via systemic administration, the loading of siRNA into the liposomal particle is one of the more desirable strategies for conferring stability in the systemic circulation, and the efficient delivery of the siRNA to a target organ (i.e. liver and tumor) [12–15].

We recently proposed a packaging concept referred to as "Programmed Packaging" [16,17], in which various types of devices

☆ Hidetaka Akita, Kentaro Kogure and Rumiko Moriguchi equally contributed to this study. These authors are listed alphabetically in accordance with family name.

☆☆ A publishers' error resulted in this article appearing in the wrong issue. The article is reprinted here for the reader's convenience and for the continuity of the special issue. For citation purposes, please use the original publication details; Journal of Controlled Release 143, pp.311-317. DOI of original item: 10.1016/j.jconrel.2010.01.012.

* Corresponding author. Laboratory for Molecular Design of Pharmaceutics, Faculty of Pharmaceutical Sciences, Hokkaido University, Kita-12, Nishi-6, Kita-ku, Sapporo, Hokkaido 060-0812, Japan. Tel.: +81 11 706 3919; fax: +81 11 706 4879.
E-mail address: harasima@pharm.hokudai.ac.jp (H. Harashima).
[1] Present address: "Kyoto Pharmaceutical University, 5 Nakauchi-cho, Misasagi, Yamashina-ku, Kyoto 607-8414, Japan".

0168-3659/$ – see front matter © 2010 Elsevier B.V. All rights reserved.
doi:10.1016/j.jconrel.2010.08.023

are incorporated into nanoparticles in a manner such that their topology is controlled. Based on this concept, multifunctional envelope-type nano-devices (MEND) were originally established for use as a plasmid DNA (pDNA) carrier. For the application of this system to siRNA delivery, nano-sized complexed cores were similarly formed with siRNA using an amphiphatic polycation (i.e. stearylated octaarginine; STR-R8), which leads to its loading in the lipid envelope by hydration methods ($MEND_{hydo}$) [18]. The outer surface of the $MEND_{hydo}$ can be modified with octaarginine (R8), which induces cellular uptake of the particle by macropinocytosis, a useful pathway that avoids lysosomal degradation.

In the present study, we report on a mechanism-based development of a siRNA delivery system, which can knockdown the gene expression at 1/10 the dose. For this purpose, a pH-sensitive fusogenic peptide was modified for endosomal escape. Furthermore, the packaging method was altered, resulting in the formation of a more homogenous and smaller particle, which is advantageous in terms of improving the intracellular dissociation process. In this development process, we made maximum use of the quantitative imaging analysis for the intracellular trafficking of siRNA (confocal image-assisted 3-dimensionally integrated quantification; CIDIQ), which provides information on the rate-limiting process of the siRNA carriers. Finally we successfully demonstrate *ex vivo* siRNA delivery to primary mouse bone marrow-derived dendritic cells (BMDCs) for potential use as a cancer vaccine.

2. Materials and methods

2.1. Materials and cell lines

1,2-Dioleoyl-*sn*-glycero-3-phosphoethanolamine (DOPE) and 4-nitrobenzo-2-oxa-1,3-diazolyl-DOPE (NBD-DOPE) were purchased from AVANTI Polar Lipids Inc. (Alabaster, AL). Cholesteryl hemisuccinate (5-Cholesten-3β-ol 3-hemisuccinate; CHEMS), ovalbumin (OVA) and lipopolysaccharide (LPS) were obtained from Sigma-Aldrich Co. (St. Louis, MO). Cholesteryl GALA (Chol-GALA) was custom-synthesized by KURABO, as reported previously [19]. Lipofectamine 2000 was obtained from Invitrogen Co. (Carlsbad, CA). The $OVA_{257-264}$ peptide (SIINFEKL) was synthesized by Kurabo Industries (Osaka, Japan). HeLa cells and E.G.7-OVA cells were purchased from RIKEN BioResource Center (Ibaraki, Japan) and the American Type Culture Collection (Manassas, VA), respectively. siRNA sequences used in the present study, and establishment of HeLa cells stably expressing luciferase (HeLa-GL3) were described in Supplemental Information.

2.2. Animals

Female C57BL/6J mice (6–8-weeks old) were obtained from CLEA Japan Inc. (Tokyo, Japan) and maintained under specific pathogen-free conditions. The use of the mice was approved by the Pharmaceutical Science Animal Committee of Hokkaido University.

2.3. siRNA-loading MENDs

The prototype R8-MEND was prepared by the hydration method (R8-$MEND_{hydo}$) as described previously [18]. The MEND prepared with another protocol (R8-$MEND_{SUV}$) was prepared by mixing small unilamellar vesicles (SUVs) with a suspension of siRNA/STR-R8. For the preparation of the SUV, lipid films containing DOPE and phosphatidic acid (PA) at a ratio of 7:2 (total lipid content: 0.55 μmol) were hydrated with 1 ml of 10 mM HEPES buffer (pH 7.4) for 10 min at room temperature. For modification of $MEND_{SUV}$ with GALA, 1 mol% of Chol-GALA was added in the lipid composition. The hydrated lipid film was then sonicated using a probe-type sonicator, and the siRNA/STR-R8 complex (33 μg siRNA/ml) was then mixed with the SUVs at a ratio of 1:2 (v/v). Finally, surfaces of $MEND_{SUV}$ were modified by adding a STR-R8 solution (10 mol% of total lipids), followed by incubation for 30 min. Gene knockdown activity of MENDs are evaluated as described in Supplemental Information.

2.4. CIDIQ analysis

The efficiencies of endosomal escape and dissociation were assessed by confocal image-based quantification as described in a recent report [20,21]. For the evaluation of endosomal escape, MENDs prepared with Alexa546-labeled siRNA was transfected to HeLa-GL3 cells. At 2.5 h after transfection, the endosomes/lysosomes were stained with Lysotracker green to discriminate between siRNA in the endosomes/lysosomes and the cytosol.

For analysis of the dissociation of the siRNA from MENDs, they were prepared with Alexa546-labeled siRNA and an NBD-labeled lipid layer. For labeling the lipid envelope with NBD, 1% of NBD-DOPE was incorporated into the lipid composition. Confocal images were captured at 9 h post-transfection, and thereafter quantitatively analyzed. Detail method for the quantitative analysis is described in Supplemental information.

2.5. Quantification of cellular uptake of MENDs by flow cytometry

The cellular uptake of the MENDs was assessed by flow cytometry. MENDs loading the Alexa546-labeled siRNA were prepared as described above. For the quantification of cellular uptake, HeLa-GL3 cells were seeded at a density of 5.0×10^4 cells per 6-well plate in the growth medium. After 24 h, the cells were incubated with the MENDs (71 nM of Alexa546-labeled siRNA) in serum-free medium for 1 h. The cells were washed once with PBS supplemented with 0.5% bovine serum albumin and 0.1% NaN_3, and then trypsinized and collected in a microtube, followed by washing two additional times by repeated precipitation of the cells by centrifugation (1500 rpm, 4 °C, 5 min) and resuspended in 1 ml of PBS including heparin (20 U/ml). Finally, the cells were suspended in 1 ml of PBS. The cell suspension was then filtered through nylon mesh to remove cell aggregates and dust, and the cells were then analyzed by flow cytometry (FACScan, Becton Dickinson).

2.6. Preparation of BMDCs of mice

BMDCs were prepared as reported previously [22] with minor modifications. Briefly, bone marrow cells were cultured for 4 h in RPMI1640 medium containing 50 μmol/l 2-mercaptoethanol, 10 mM HEPES, 1 mM sodium pyruvate, 100 U/ml penicillin–streptomycin, and 10% fetal calf serum. Non-adherent cells were harvested and cultured in the same medium supplemented with 10 ng/ml GM-CSF (R&D Systems, Basel, Switzerland). On days 2 and 4, non-adherent cells were removed, and adherent cells were cultured in fresh medium containing 10 ng/ml GM-CSF. On day 6, non-adherent and loosely adherent cells were used as immature DCs. Cell surface expression of CD11c in more than 85% of the cell population was confirmed by flow activated cell sorting (FACS) analysis.

2.7. Evaluation of gene knockdown activity of MENDs in BMDCs

To evaluate the silencing effect against GAPDH, BMDCs (1.2×10^6 cells) were incubated with R8/GALA-$MEND_{SUV}$ loading 60 pmol siRNA for 2 h at 37 °C in 0.5 ml of serum-free OPTI-MEM I containing 10 ng/ml GM-CSF in 12-well plate. Then, 1 ml of RPMI1640 medium containing GM-CSF was added to the cells, and incubated further 22-h incubation.

In the case of SOCS1 knockdown, BMDCs were transfected with R8/GALA-$MEND_{SUV}$ containing 40 pmol siRNA for 2 h. RPMI1640 medium containing GM-CSF was then added to the cells, followed by further 2-h incubation. BMDCs were washed and incubated in the fresh medium for 2 h at 37 °C and then stimulated with IFN-γ (50 ng/ml) for 24 h. SOCS1 expression in BMDCs is evaluated as described in Supplemental Information.

2.8. Quantification of cytokine production from BMDCs

Non-treated or siRNA-transfected BMDCs were stimulated with IFN-γ (50 ng/ml) for 24 h. Concentrations of TNF-α and IL-6 in the culture supernatants were measured by Quantikine (R&D Systems).

2.9. DC immunization and tumor challenge

Immature BMDCs transfected with control siRNA or anti-SOCS1 siRNA were pulsed with OVA peptides (0.5 μM) and OVA protein (50 μg/ml) at 37 °C for 30 min, followed by stimulation with LPS (0.5 μg/ml) for 1 h to develop mature BMDCs. Then, 3.8×10^5 cells were washed with PBS to remove extracellular LPS, and injected into the hind footpads of C57BL/6 mice. One week after immunization, 8×10^5 E.G.7-OVA cells were inoculated subcutaneously into the right flank of immunized mice. Tumor volume was calculated by the following formula: (major axis × minor axis^2) × 0.52.

3. Results

3.1. Gene knockdown activity of MENDs

We wish to report herein on a siRNA delivery system that is effective at low dose, and its development processes with the aid information concerning intracellular trafficking. The carrier was applied to the *ex vivo* gene knockdown of SOCS1 in BMDCs to enhance the effect of a cancer vaccination. Since the siRNAs are incorporated into Argonaute 2 (AGO2) and the RNAi-induced silencing complex (RISC) is in the cytosol, the disposition of siRNA in the cytoplasmic region strongly reflects the efficiency of siRNA. BMDC is not appropriate for the imaging analysis of intracellular trafficking of siRNA, since the volume of the cytoplasmic region is small. Therefore, we first improved the carriers using HeLa-GL3 cells.

In initial experiments, the gene knockdown activity of prototype R8-MEND prepared with hydration method (R8-MEND$_{hydo}$) was evaluated (Fig. 1a). The R8-MEND$_{hydo}$ was found to have a strong gene knockdown effect (>75%) against a HeLa-GL3 at a concentration of approximately 120 nM. However, when the dose was decreased, the gene knockdown effect gradually decreased, with an IC_{50} of approximately 75 nM, and eventually decreased to >10% at 1/10 of the original dose. To achieve a promising breakthrough, the gene knockdown efficiency per 1 particle of siRNA carrier must be substantially improved in order to achieve minimum clinical dosing to avoid any undesirable side effects.

To clearly show the stepwise upgrading of MENDs, the knockdown efficiencies of MENDs in final form (R8/GALA-MEND$_{SUV}$; red bar), and in intermediate forms (blue and yellow bars) at low dose (12 nM) are summarized in Fig. 1b. Improving cytoplasmic delivery, endosome-fusion and/or disruption efficiency are commonly employed tactics. One such membrane-fusion inducer is GALA [23–25], a pH-dependent fusogenic peptide, which induces loaded cargos to be released into the cytosol [19,26]. For the surface display of GALA in a lipid envelope, Chol-GALA was then incorporated at 1 mol% of total lipid [19]. In addition, we recently demonstrated that R8-modified liposomes composed of DOPE/PA = 7/2 are capable of enhancing the cytoplasmic delivery of macromolecules derived from its highly fusogenic activity to endosomes [27,28].

In the light of these previous achievements, R8-MENDs were prepared with a lipid composition of DOPE/PA = 7/2 plus 1% Chol-GALA (R8/GALA-MEND$_{hydo}$). Gene knockdown activity was evaluated at 1/10 of the dose (12 nM), where the gene knockdown effect was negligible in the case of a conventional R8-MEND$_{hydo}$ composed of DOPE/CHEMS (Fig. 1b; black bar). However, regardless of these modification, gene knockdown activity continued to be marginal (approximately 15%, Fig. 1b; blue bar).

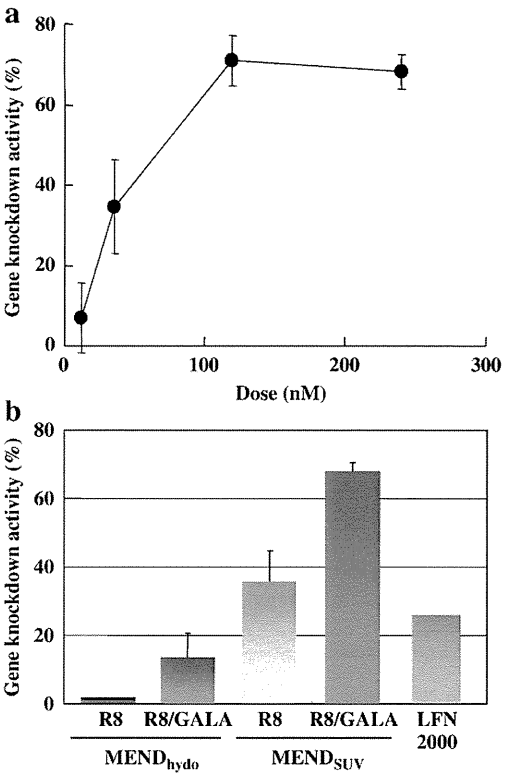

Fig. 1. Gene knockdown activity of MENDs. Function of R8- and R8/GALA-MENDs prepared with hydration method and SUV-mixing method. a. Dose-dependent knockdown effect of the luciferase gene by a prototype R8-MEND$_{hydo}$. MENDs loading siRNA against GFP or luciferase were incubated with HeLa-GL3. Gene knockdown activity was calculated as the percentage of decrease in luciferase activity in the anti-luciferase siRNA treatment to that for the anti-GFP siRNA treatment. b. Silencing effect of MEND$_{hydo}$ and MEND$_{SUV}$ loading anti-luciferase siRNA on luciferase activity of HeLa-GL3. siRNA-loading MENDs with or without GALA modification were added to HeLa-GL3 cells at 12 nM siRNA for 24 h. Luciferase activities were measured as described in Methods. Data are represented as the mean ± SD.

Here, we wish to report that siRNA activity can be dramatically improved by modifying the method used to prepare the MEND (R8/GALA-MEND$_{SUV}$). The positively charged siRNA/STR-R8 complexed core is incubated with negatively charged small unilamellar vesicles (SUVs) composed of DOPE/PA = 7:2 plus 1 mol% of Chol-GALA. The surface of the resulting particles is then modified with STR-R8. As a result, the R8/GALA-MEND$_{SUV}$ particles are smaller in size, compared to the R8/GALA-MEND$_{hydo}$. Furthermore, the polydispersity index of the MEND$_{SUV}$ preparation is smaller, suggesting that the sizes of the prepared MENDs are more uniform (Table 1). The most significant finding is that the knockdown effect was dramatically increased to more than 70% (Fig. 1b, red bar) even at 1/10 the dose, indicating that the knockdown efficiency per 1 particle of siRNA was successfully improved by 10 times. When the GALA modification was not employed (R8-MEND$_{SUV}$), the knock down activity was reduced to 40% (Fig. 1b, yellow), suggesting that GALA modification of the MEND$_{SUV}$ is a valid strategy for the efficient cytoplasmic delivery of siRNA. At this dosage, LFN2000 showed only a slight gene knockdown

Table 1
Physicochemical characteristics of MENDs.

	R8-MEND$_{hydo}$	R8/GALA-MEND$_{hydo}$	R8/GALA-MEND$_{SUV}$
Size (nm)	172.8	178	131.5
Z-potential (mV)	52.5	47.4	42.6
PDI	0.25	0.26	0.17

effect (Fig. 1b, green), suggesting that the R8/GALA-MEND$_{SUV}$ is a highly efficient gene knockdown system. The key to the success of this strategy can be attributed to the quantitative analysis of the intracellular trafficking of siRNA as described in the following sections.

3.2. Evaluation of endosomal escape efficiency

In the present study, the intracellular trafficking of MENDs was evaluated by means of confocal image-assisted 3-dimensionally integrated quantification (CIDIQ; Fig. 2a) [20,21]. Cells were transfected with R8-MEND$_{hydo}$ loading Alaxa543-labeled siRNA, and the endosome/lysosome fraction was then stained with Lysotracker Green at 2.5 h post-transfection. Z-series of images were then captured by confocal laser scanning microscopy (Fig. 2b and c for R8-MEND$_{hydo}$ and R8/GALA-MEND$_{hydo}$, respectively). As a result, siRNA were detected as clustered forms, as shown in Fig. 2b. The siRNA signals colocalized with Lysotracker Green (yellow clusters) are denoted as siRNAs in endosomes/lysosomes. In addition, the siRNAs signals that are not colocalized with Lysotracker Green (red clusters) are denoted as those that escaped from endosome/lysosomes. For quantification, the pixel areas of the siRNA clusters detected in the cytosol (red clusters) and in endosomes/lysosomes (yellow clusters) were separately integrated through all of the Z-series of images (S (red) and S(yellow), respectively). Endosomal escape efficiency was denoted as S(red) divided by the total of S(red) and S(yellow). The calculated endosomal escape efficiency of R8-MEND$_{hydo}$ in 15 individual cells indicated that an average endosomal escape efficiency of 52.4% (Fig. 2d). In contrast, siRNA were observed to be predominant in the cytosol in some cells (Fig. 2c) in R8/GALA-MEND$_{hydo}$. Quantitative evaluation showed that the endosome escape efficiency was increased to an average of approximately 70% (Fig. 2d). The enhanced endosomal escape efficiency may be responsible for the slight improvement in gene knockdown activity (Fig. 1d; blue bar). However, the discrepancy between the slight gene knockdown effect and the high (approx.70%) endosomal escape efficiency (Fig. 2d) indicates that another process must be overcome for the successful development of an efficient siRNA delivery system.

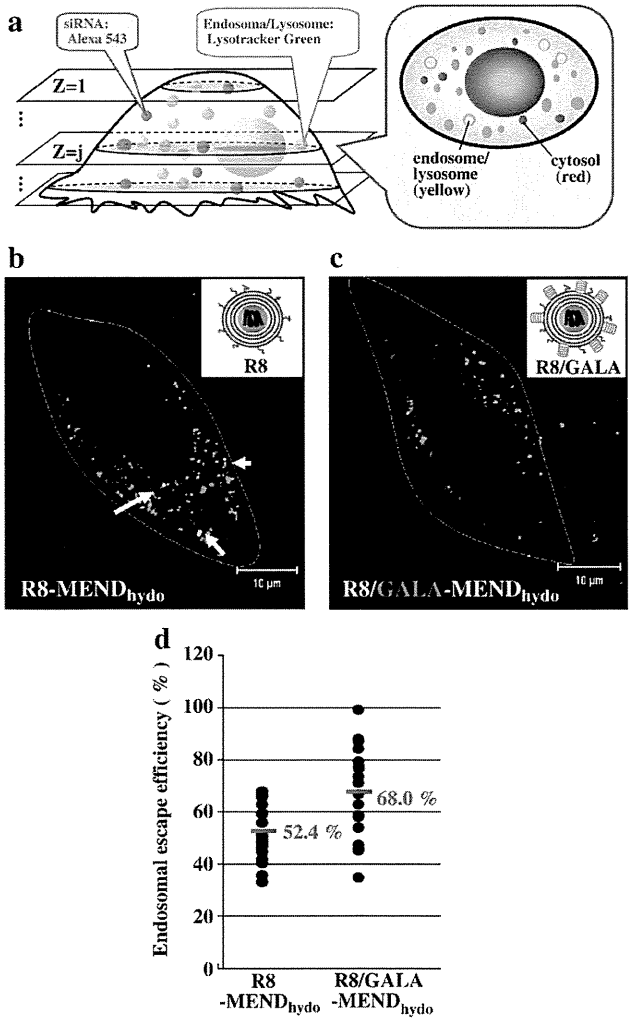

Fig. 2. Evaluation of endosomal escape efficiencies of siRNA. Evaluation of endosomal escape efficiency of MENDs. a. Schematic diagram illustrating the quantitative evaluation system used to evaluate endosomal escape. MENDs prepared with Alexa546-labeled siRNA were transfected to HeLa-GL3 cells. The endosomes/lysosomes were stained with Lysotracker green to discriminate between pDNA in endosomes/lysosomes and the cytosol. The fraction of siRNA in endosomes and the cytosol was quantified based on the pixel area of clusters in each region of interest, as described in Methods. b–c. Typical confocal image of intracellular trafficking of R8-MEND$_{hydo}$ with (c) or without (b) GALA modification. White lines indicate the cellular region. Green, red and yellow (indicated by arrowhead) represents endosome/lysosome, siRNA in the cytoplasm and siRNA in endosomes/lysosomes, respectively. d. Quantitative comparison of endosome escape efficiency between GALA-modified and unmodified R8-MEND$_{hydo}$. Endosome escape efficiency in 15 individual cells was plotted.

3.3. Evaluation of cellular uptake and intracellular dissociation efficiency

It is postulated that cytoplasmic dissociation process of siRNA is also rate-limiting for its function. The dissociation efficiency of siRNA in R8/GALA-MEND$_{hydo}$ was quantified by CIDIQ analysis (Fig. 3a). Alexa546-labeled siRNA was loaded in the MEND$_{hydo}$, with a labeling of lipid envelope by 1 mol% NBD. The dually labeled R8/GALA-MEND$_{hydo}$ was transfected, and a Z-series of confocal images were then captured at 9 h post-transfection (Fig. 3a). siRNA in loaded and dissociated form were detected as yellow clusters and red clusters, respectively (Fig. 3b). The pixel areas corresponding to the red and yellow clusters were integrated using all of the Z-series of confocal images (S(red) and S(yellow), respectively). Dissociation efficiency was denoted as the percentage of S (red) to the total of the S(red) and S(yellow) clusters. Quantification of the pixel areas of the clusters indicated that only 56% of the siRNA was dissociated in the R8/GALA-MEND$_{hydo}$ (Fig. 3d). In contrast, almost all of the siRNA were detected as red clusters in the case of the R8/GALA-MEND$_{SUV}$ (Fig. 3c). A quantitative evaluation indicated that the dissociation efficiency for the R8/GALA-MEND$_{SUV}$ was approximately 90% (Fig. 3d). Furthermore, the dissociation efficiency was homogenous over the cell population. A FACS analysis revealed that the cellular uptake varied substantially from one cell to another in R8-MEND$_{hydo}$ and R8/GALA-MEND$_{hydo}$. On the other hand, the cellular uptake efficiencies for the MEND$_{SUV}$ were slightly higher (at maximum of 2-fold by geo mean calculation) and more homogeneous for individual cells. Collectively, controlling the number of lipid layers is an advantage, in terms of improving dissociation efficiency, and for overcoming heterogeneity in the cellular uptake process (Fig. 3d and e).

3.4. Delivery of anti-SOCS1 siRNA to BMDCs for cancer immunotherapy

To investigate the utility of the R8/GALA-MEND$_{SUV}$ in the delivery of therapeutic siRNAs, we examined the biological response of a gene knockdown targeting SOCS1 in mouse bone marrow-derived dendritic cells (BMDCs). In order to confirm the RNAi efficacy in these cells, anti-GAPDH siRNA was transfected to BMDCs for 24 h. The R8/GALA-MEND$_{SUV}$ was able to suppress GAPDH expression more prominently than LFN2000 (Supplemental Fig. 1). We subsequently examined the silencing effect against SOCS1 following induction by IFN-γ. As shown in Fig. 4a, SOCS1 mRNA was reduced to 21.5% of the levels of non-treated BMDCs. As expected, BMDCs transfected with anti-SOCS1 were more responsive to IFN-γ than those transfected

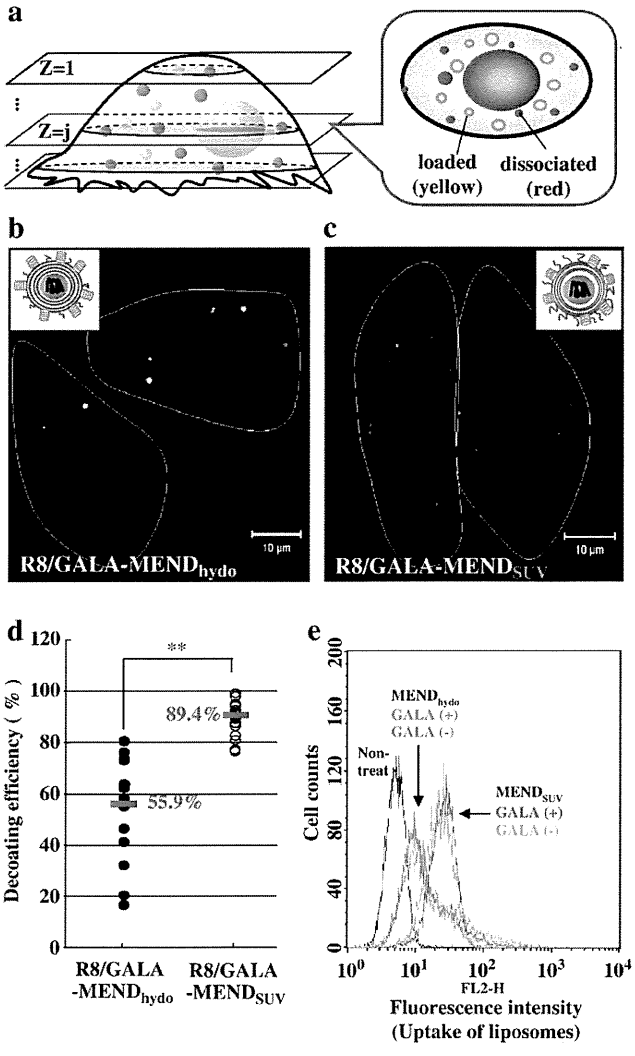

Fig. 3. Evaluation of dissociation efficiencies of siRNA. Comparative evaluation of cellular uptake and dissociation efficiency between GALA-modified R8/GALA-MEND$_{hydo}$ and R8/GALA-MEND$_{SUV}$. a. Schematic diagram illustrating the system used to evaluate the dissociation process. MENDs were prepared with Alexa546-labeled siRNA. The lipid envelope was labeled by incorporation of an NBD-labeled lipid. Fraction of siRNA in the dissociated form was quantified based on the pixel area of clusters in each region of interest as described in Methods. b–c. Typical confocal images of R8/GALA-MEND$_{hydo}$ (b) and R8/GALA-MEND$_{SUV}$ (c). White lines indicate the cellular region. Red and yellow clusters represent dissociated and loaded siRNA, respectively. d. Comparison of dissociation efficiency between R8/GALA-MEND$_{hydo}$ and R8/GALA-MEND$_{SUV}$. Dissociation efficiency in 15 individual cells was plotted. e. Evaluation of the cellular uptake of siRNA introduced by a conventional MEND$_{hydo}$ and the MEND$_{SUV}$. MENDs loading Alexa546-labeled siRNA were incubated with HeLa-GL3 cells for 1 h, and then subjected to flow cytometry.

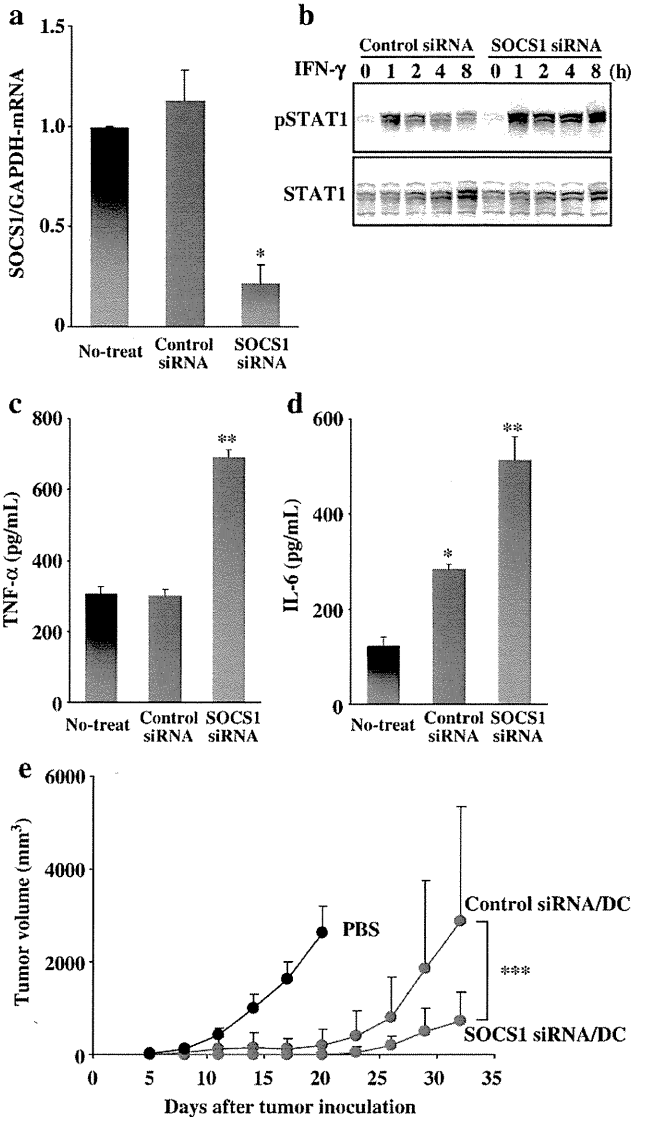

Fig. 4. SOCS1 gene silencing and antitumor activity. SOCS1 gene silencing and enhancement of antitumor activity of dendritic cells mediated by R8/GALA-MEND$_{SUV}$. a. Gene silencing of SOCS1. BMDCs were transfected with anti-SOCS1 siRNA or negative control siRNA. Six hours after transfection, the cells were stimulated with IFN-γ for 24 h and assayed for mRNA expression by quantitative RT-PCR. SOCS1 levels were normalized to non-treated BMDCs. Data are mean ± S.D. of three independent experiments. *P<0.005 vs. Control siRNA. b. STAT1 tyrosine phosphorylation in anti-SOCS1 siRNA or negative control siRNA-transfected BMDCs stimulated with IFN-γ was analyzed by Western blotting. c–d. TNF-α (c) and IL-6 (d) concentrations in the culture supernatants were determined by ELISA at 24 h after stimulation with IFN-γ. Data are the mean ± S.D. of three independent experiments. *P<0.005, **P<0.001 vs. non-treated BMDCs. e. Inhibition of E.G.7-OVA tumor growth by SOCS1-silenced BMDCs immunization. C57BL/6 mice (4 mice/group) were immunized with 3.8×10^5 siRNA-transfected, OVA-pulsed BMDCs. One week after DC immunization, 8×10^5 tumor cells were inoculated s.c. and tumor size was measured at 3 day intervals. ***P<0.005 vs. Control siRNA/DC.

with control siRNA, as evidenced by the enhanced and prolonged phosphorylation of STAT1 (Fig. 4b). Consistent with these data, higher levels of proinflammatory cytokines (i.e. TNF-α and IL-6) were produced by the SOCS1-silenced BMDCs upon stimulation (Fig. 4c and d, respectively). We observed a slight increase in IL-6 production by BMDCs transfected with control siRNA. This is probably due to sequence-dependent non-specific stimulation by siRNA transfection, since a similar increase in IL-6 was also observed with different siRNAs.

The effect of SOCS1 knockdown on the ability of BMDCs to induce antitumor immunity was then examined (Fig. 4e). BMDCs transfected with SOCS1-targeting or control siRNA were pulsed with an antigen (OVA). These pulsed BMDCs are activated by adjuvant (LPS), and then pre-immunized to C57BL/6 mouse. These mice were challenged with E.G.7-OVA tumor cells one week after the immunization. BMDCs vaccination effectively retarded tumor growth regardless of SOCS1 knockdown compared with control mice treated with PBS until 20 days. After a longer evaluation, however, SOCS1-silenced BMDCs were more potent in suppressing tumor growth compared to the control BMDCs. These results show that siRNA loaded in R8/GALA-

$MEND_{SUV}$ can efficiently suppress endogenous gene expression and consequently enhance dendritic cell-based vaccine potency *in vivo*.

4. Discussion

In the present study, we report on the successful development of an efficient siRNA carrier (R8/GALA-$MEND_{SUV}$) which is applicable to manipulating the function of BMDCs. In this improvement process, quantitative information concerning the intracellular trafficking of siRNA was used to clarify the drawbacks of the carriers that needed to be overcome. It has been reported that siRNA is rapidly degraded in the cytosol [29]. Therefore, the efficiencies of endosomal escape and dissociation were quantified at an earlier time post-transfection (2.5 h and 9 h. respectively) to minimize the effect of siRNA degradation, while gene knockdown activity was evaluated at 48-h post-transfection.

Concerning endosomal escape, we recently demonstrated that R8-modified liposomes composed of DOPE/PA = 7/2 are capable of enhancing the cytoplasmic delivery of encapsulated molecules derived from its high fusogenic activity to endosomes [28]. Since the replacement of R8 with octa-lysine (K8) diminished the gene knockdown activity of siRNA due to a decrease in membrane-fusion efficiency at acidic pH used, R8 and the lipid composition may synergistically function in membrane fusion. Moreover, we also demonstrated that the surface modification of GALA, a pH-sensitive fusogenic peptide permits an enhanced endosomal escape in response to the low pH in endosomes [19,23,24]. In spite of these combinatorial devices, the only a slight gene knockdown effect (Fig. 1d; blue bar) was observed even in R8/GALA-$MEND_{hydo}$ with a high (approx. 70%) endosomal escape efficiency (Fig. 2). This indicates that an improvement in endosomal escape is not sufficient for effective siRNA delivery.

Since endosomal escape is coupled with a membrane fusion, it is expected that particles are released to the cytosol as a dissociated form. However, as observed in MENDs encapsulating pDNA, electron microscopic observations showed that the MENDs prepared with lipid hydration has a multi-lamellar membrane structure [27]. Therefore, we hypothesized that siRNA was released into the cytosol while still associated with excess amount of lipid envelope, and thus fails in effective gene knockdown. Importance of dissociation processes in the effective function of cargo was also shown in a pDNA-loading MEND. It was recently demonstrated that the incorporation of short PEG-modified lipids (i.e. tetraethyleneglycol (TEG)-conjugated cholesterol) is useful in controlling the number of lipid envelopes, resulting in an improvement in particle uniformity with a reduced particle size. The TEG-modified lipid particles can enhance not only cellular uptake, but also transcription activity by improving intracellular decoating, resulting in an improvement in transfection activity of more than 100-fold [30]. Although the structure of the R8/GALA-$MEND_{SUV}$ prepared with siRNA core remains to be clarified, we hypothesize that the negatively charged SUVs may be assembled around the positively charged core, and then triggers the encapsulation of the core complex through membrane fusion with neighboring SUVs to confer the coating with the di-lamellar endosome-fusogenic lipid envelope (Supplemental Fig. 2). The particle formation of di-lamellar envelope structure by incubation with pDNA core and liposomes has also been proposed previously [31]. Then, similar to this TEG-modified pDNA particle, coating with a limited amount of endosome-fusogenic lipid envelope may facilitate the intracellular decoating of the siRNA particle, triggered by the membrane fusion of the envelope with endosomes. While cellular uptake was slightly improved in the case of the R8/GALA-$MEND_{SUV}$ compared with the R8/GALA-$MEND_{hydo}$, the extent (at a maximum 2 fold) is not sufficient to explain the effective gene knockdown at 1/10 of the dose. The efficient dissociation of siRNA in the R8/GALA-$MEND_{SUV}$ in comparison with R8/GALA-$MEND_{hydo}$ (Fig. 3) is a key process for improving gene knockdown efficiency. It is plausible, however, that the surface modification of an endosome-fusogenic peptide (GALA) on a limited number of envelopes is advantageous for the dissociation of siRNA from the carriers, this would be coincident with endosomal escape.

As antigen presenting cells, DCs play a crucial role in the initiation of an immune response and the regulation of cell-mediated immune reactions. Genetic modification of DCs has been demonstrated to be effective for cancer immunotherapy. One of the strategies for achieving this is to enhance the life-span of DCs by the introduction of antiapoptotic genes (Bcl-X_L and Bcl-X_{FNK}) genes [32] or the gene knockdown of apoptotic genes (Bak and Bax) [33]. Extension of the life-span is correlated with enhanced vaccine efficiency. Another strategy would be to knockdown immunosuppressive proteins [7,8]. As a demonstration of the potential utility of R8/GALA-$MEND_{SUV}$ in *in vivo* use, siRNA targeting SOCS1, was introduced to the BMDCs and enhanced immunoresponse against cancer (Fig. 4). BMDCs transfected with anti-SOCS1 showed more effective tumor growth inhibition compared with those treated with control siRNA. However, even in the SOCS1-knockdown group, significant tumor growth starts to appear at 20 days after tumor inoculation. While the mechanism for the loss of function has not been clarified, one of the most plausible reasons is the short half-life of the DCs. A combination of SOCS1 gene knockdown and extending the half-life of DCs by the introduction of antiapoptotic genes [32] or the gene knockdown of apoptotic genes [33] may lead to a more potent and more long-lasting tumor vaccination system.

Currently many experiments are being conducted with cationic liposome-based transfection reagents including LFN2000. However, the introduction of nucleic acids such as plasmid DNA and siRNA into *ex vivo* cultured DCs appears to be difficult. In addition, some cationic lipids have immunostimulating activity which might cause undesirable side effects. Yan et al. showed that a cationic lipid (i.e. DOTAP), stimulates BMDCs through the generation of reactive oxygen species (ROS) and induces chemokine, cytokine and co-stimulatory molecules (CD86/CD80) [34]. The DOTAP liposome showed *in vivo* antitumor effects by lipid itself at an optimal dose. On the other hand, high levels of DOTAP-generated ROS cause apoptosis in dendritic cells. Therefore, an effective and substantially non-stimulating delivery system would be highly desirable. In a previous study, Nakamura et al. reported that R8-modified liposomes did not show non-specific antitumor effects *in vivo* [35]. Therefore, the R8/GALA-MEND system was expected to have minor immunostimulatory effects. We recently demonstrated that the encapsulation of OVA in R8-modified liposomes drastically inhibits E.G.7-OVA tumor growth after subcutaneous immunization, compared with that for an OVA solution [35]. A combination of antigen delivery and regulation of the signaling pathway by siRNA delivery with R8-modified particles may prove to be an innovative cancer vaccine.

In summary, a quantitative evaluation of intracellular trafficking revealed that dissociation, as well as the endosome escape process is significant rate-limiting processes for siRNA. GALA modification and reducing the number of lipid envelopes contribute to the successful improvement of the siRNA carrier, which can be applied to BMDC for *ex vivo* cancer vaccine.

Acknowledgements

This work was supported by CREST from the Japan Science and Technology Agency (JST), Grant for Industrial Technology Research from the New Energy and Industrial Technology Development Organization (NEDO) and in part by the Japan Society for the Promotion of Science. The authors thank Dr. Milton S. Feather for his helpful advice in writing the English manuscript.

Appendix A. Supplementary data

Supplementary data associated with this article can be found, in the online version, at doi:10.1016/j.jconrel.2010.08.023.